QUANTUM THEORETICAL STUDY ON CURRENT-VOLTAGE CHARACTERISTICS IN MOLECULAR TRANSPORT PHENOMENA

SAWANYA SUWANNAWONG

SEPTEMBER 2016

QUANTUM THEORETICAL STUDY ON CURRENT-VOLTAGE CHARACTERISTICS IN MOLECULAR TRANSPORT PHENOMENA

A dissertation submitted to

THE GRADUATE SCHOOL OF ENGINEERING SCIENCE

OSAKA UNIVERSITY

in partial fulfillment of the requirements for the degree of

DOCTOR OF PHILOSOPHY IN ENGINEERING

by

SAWANYA SUWANNAWONG

SEPTEMBER 2016

Abstract

Nowadays, scientific issues have been focused on nanotechnology and properties of particular particle transport phenomena, and thus, atomistic-scale computations have been utilized in various research fields of physics, chemistry, biology, materials sciences, and engineering applications. In this thesis, we have developed a theoretical model to distinguish electrical conductance of molecular species in terms of current-voltage (I-V) characteristics. A novel method to evaluate non-equilibrium electronic processes is proposed, which may overcome a computational barrier limited in ground states. Some numerical results from ab initio computations are also demonstrated, focusing on the orientation of molecules to the electrode surfaces in non-equilibrium transport processes, such as single-molecule junctions and oxygen reduction reactions (ORR). Our theoretical model is developed based on the Heisenberg uncertainty principle and numerical procedures in density functional theory. Further computations have been carried out to investigate a relationship between the orientation of dipole moment and energy levels in molecules under the external electric field. Firstly, the present method is applied to a single-molecule junction in deoxyribonucleic acid (DNA) sequencing technique by using nano-gapped sensing electrodes, where four types of DNA bases can be identified by tunneling current measurement associated with the unique conduction property of each base. Sequential identification of DNA bases by measuring their electrical conductance is one of the most interesting topics, because it is expected to reduce the time and cost for sequence analyses for gene therapy, safety of foods, and

criminal investigations. In the present study, electric current responses are evaluated as a function of rotation angles defined along a chemical bond between the sugar and base. It is found that orientations of molecular orbitals to the electric fields result in differences in the dipole moments and in the energy changes. As a result, the computed electrical conductance is in reasonable agreement with the previous results from both experimental and theoretical approaches by other groups. In another topic, we apply our developed method to ORR observed in proton exchange membrane fuel cells that have attracted significant attention as an alternative energy source, owing to their low operating temperature and applicability in both stationary and portable uses. Such clean energy sources are expected to be a promising solution to overcome several problems in the worldwide energy crisis and environment pollution. For the wide area use, however, the most critical problem is the high production cost and the high overpotential which is principally caused by ORR. The ORR is a complicated interfacial reaction which includes various possible intermediate pathways depending on the adsorption and dissociation of molecules. There have been numerous studies about ORR using various computational methods; however, previous works seem to propose contradictory conclusions due to the different computational procedures and limitations in different frameworks. Although most of the results may usefully provide the detail of ORR mechanism and discuss the possibility of each pathway regarding to the activation energies, non-equilibrium electronic process has not been explained enough. In this study, focusing on the interaction between dissociatively adsorbed molecules and catalyst surface, the I-V characteristics are evaluated for each possible adsorption pathway. Our model can sense the difference in the geometrical configurations from the viewpoint of non-equilibrium electronic process. Furthermore, the *ab initio* molecular dynamics simulations are performed to simulate the dynamical

behavior of an adsorbed molecule to the modeled surface, and electrical profiles are also proposed as a novel approach to describe the charge transport in ORR.

Table of contents

Chapter 1

General Introduction

1.1 Atomistic Computations of Non-equilibrium Electron Transport

In nanotechnology, the electron transport has been emphasized in various fields of physics, chemistry, biology, materials science and engineering technology. Due to the atomistic scale, experimental methods are limited to explain some problems, hence, the atomistic computations become one of the interesting topics in order to attempt to clarify this complicated mechanism. Based on the principle of consideration, the molecular calculation can be divided into two major approaches. One is a conventional molecular dynamics simulation that computes the physical movement of particles in the force field by solving the Newton's equations of motion numerically. The other is the computational quantum mechanical modelling which solves the Schrödinger equation to evaluate the static properties. Moreover, the quantum mechanics procedures provide more accuracy, since it treats the electron as the matter wave or density cloud, hence, the recent works have been performed by the quantum-based computations. Therefore, the basic knowledge is mainly discussed in this topic.

The quantum computations mostly are performed self-consistently without any empirical parameters. They also can be called as *ab initio* or first principles calculation. In quantum point of view, the fundamental interaction is the Schrödinger equation. It is a mathematical derivation of energies and orbitals to obtain the geometry and electronic structures. In stationary and non-relativistic terms, it can be written in simple form as Eq. (1.1) [1]:

$$H\psi = E\psi \tag{1.1}$$

where E is the energy eigenvalue of electron. ψ is the wave function that is defined by the mathematical function to explain the wavelike nature of electron. H is a Hamiltonian operator that is a set of mathematical operations to compute the total of kinetic and potential energy of electrons within the atoms. The Hamiltonian can be mathematically derived as:

$$H = -\sum_i \frac{\hbar^2}{2m_\mathrm{e}}\nabla_i^2 - \sum_k \frac{\hbar^2}{2m_k}\nabla_k^2 - \sum_i \sum_k \frac{e^2 Z_k}{4\pi\epsilon_0 r_{ik}} + \sum_{i<j} \frac{e^2}{4\pi\epsilon_0 r_{ij}} + \sum_{k<l} \frac{e^2 Z_k Z_l}{4\pi\epsilon_0 r_{kl}} \tag{1.2}$$

where i and j represent the number of electron and k and l are those of nuclei, $\hbar$ is divided Planck's constant, m_e is the mass of the electron, m_k is the mass of nucleus k, e is the electric charge of electron, Z is the atomic number, ϵ_0 is the electrical permittivity of space and r represents the distance between particles. ∇^2 is the Laplacian operator of the coordiante system [1].

There are two major methods to solve the Schrödinger equation that are wave function-base method, i.e. Hartree-Fock approximation, and density-based method what usually called as density function theory (DFT). The DFT approach employs the electron density as the basic variable, thus being able to treat larger-scale model and increasing the degree of accuracy. The basic idea of DFT is to reformulate the energy

of system as a function of electron density instead of the electron wave function. The electron density which is the function of space and time is treated as the fundamental property to fasten the time of many-body analysis. The Hohenberg and Kohn theorem [2] stated that the electron density determines the ground state properties of systems, so that the total energy of many-electron systems can be computed according to the density functional.

As in flow chart of Kohn-Sham SCF method (Figure 1.1) [1], a self-consistent field (SCF) iteration is carried out by using a finite basis set which is a mathematical function relating to the molecular orbitals, then, the Kohn-Sham equation [3], which writes the function of energy as molecular orbitals to express the kinetic energy and the density of other components, is solved in order to evaluate the converged value of the electron density and total energy [1]. This procedure corresponds to find out the optimized electron density and other physical properties. Beside the mathematical calculation issue, the configuration of computational structure is also vital topic as in the beginning step of flow chart (Figure 1.1). To study the surficial geometry theoretically, there are two approaches to imitate the molecular structure and the environment, a slab model and a cluster approximation [4]. The slab approach applies the periodic boundary condition with bulk of surfaces separated by vacuum region; meanwhile, the cluster approach uses a few atoms standing for practical surface. To define the basis set, it is also depended on the type of the surface model ,that is, the plane wave basis set for the slab model and the localized basis set for cluster approach.

Furthermore, to calculate the motion of particles with static properties computed within the quantum mechanics, the molecular dynamics should be taken into account, hence, the *ab initio* molecular dynamics (AIMD). The AIMD simulation were introduced to elucidate electronic structures, charge distributions and interactions of molecules from both quantum and classical mechanics. This approach is used in

derivation of macroscopic motion of various particles under the controlled condition within the simulation. For treating atom, the microscopic trajectory of each individual atom in the system is determined by integration of Newton's equations of motion. At every time step of the MD simulation, the electronic structure is generated by the force acting on particles derived from a quantum based calculation, e.g., DFT method. Consequently, many-body electron systems can be analyzed by more accurate description of thermodynamic properties, phase stability, atomic dynamics, and chemical reactions. Some applications which are principally relied on the electron transport require both molecular dynamics and *ab initio* procedures to elucidate simple understanding because their mechanisms are too complicated to be studied in detail by the experiment as well as the macroscopic model. Examples of these researches include the tunneling electron via weak coupling metal-molecule in the single-molecule junctions and the redox reaction at the electrode surface in electrochemical cells [5].

The individual single molecule has been studied in both experiments and quantum computations due to its applicable use in the nanoelectronic devices, such as functional thin films and nanowires [6]. The major interesting points of these research fields are the theoretical understanding of transport phenomena in atomistic level as well as the achievement of experimental approach which leads to the commercial molecular electronic devices. In simple configuration, the single molecular junction essentially consists of two faced electrodes and a molecule as illustrated in Fig.1.2. Under applied electric field, the molecule has physical or chemical adsorption on the electrodes depending on their interaction and species, thus, the molecular junction. Electrons can propagate from one electrode to the other through in-between molecule, therefore, this molecule shows capacitance. This refers to the tunneling current in quantum mechanics. In validation of application based on such electron flow, the current-voltage (I-V) characteristics is an effective procedure, however, due to time-consuming in

practical analysis such as using controllable break junction [7], the theoretical model was proposed. Numerous works based on DFT have been studied using several basic computations such as a non-equilibrium Green's function [8, 9], a Laudauer-like formula using scattering-state approach [10], and the simple uncertainty principle associating with electronic structure calculation [5, 11, 12].

In addition, the molecular calculations also have been performed for various electrochemical reactions. One of the captivating topics is the oxygen reduction reaction (ORR) that is the rate-determining step of the proton exchange membrane fuel cells (PEMFCs). To evaluate their performance, the external electric field is applied to generate computational results such as I-V characteristics, hence the non-equilibrium study can be applied in such system. Furthermore, as shown in Fig.1.3, the ORR occurs on the catalyst surface of cathode, i.e. carbon-supported platinum, and includes the proton and electron transfer which requires quantum computations. However, most previous works focused in the view point of energy terms such as potential energy surface (PES) that illustrates the potential energy along to the structural change. Typically, it can provide a promising reaction path by comparison the energy barrier and other properties [1, 13, 14]. The electrical profile is still limited to explain by these successful works.

1.2 Objectives of the Present Study

In this study, a theoretical model has been developed to evaluate electrical conductance of molecular species in terms of I-V characteristics for the non-equilibrium electron transport. Although, various computations have been proposed, the dominance of molecular orbital and molecular dipole moment is restricted to describe. Chapter 2 provides the information of the developed theoretical model and involved theories, that

is, Heisenberg uncertainty principle and numerical procedures in *ab initio* computations. Furthermore, the background understanding of the metal-molecule junction is discussed.

Firstly, our computational approach is applied to a single-molecule junction in deoxyribonucleic acid (DNA) sequencing technique by using nano-gapped sensing electrodes which can distinguish types of DNA bases practically by unique conductance. The validity of present model is also approved by acceptable agreement with previous study as detailed in Chapter 3.

Thereafter, the study of the dissociative adsorption of oxygen molecule near biased platinum surfaces, which is a major initial sub-step of ORR, by developed theoretical model is carried out in Chapter 4. Furthermore, the *ab initio* molecular dynamics simulations are performed to simulate the dynamical behavior of an adsorbed molecule to the modeled surface, and electrical profiles are also proposed as a novel approach to describe the charge transport in ORR.

Chapter 5 presents the general conclusion of the present study. This chapter summarizes the performance of the theoretical model and recommends potential future works.

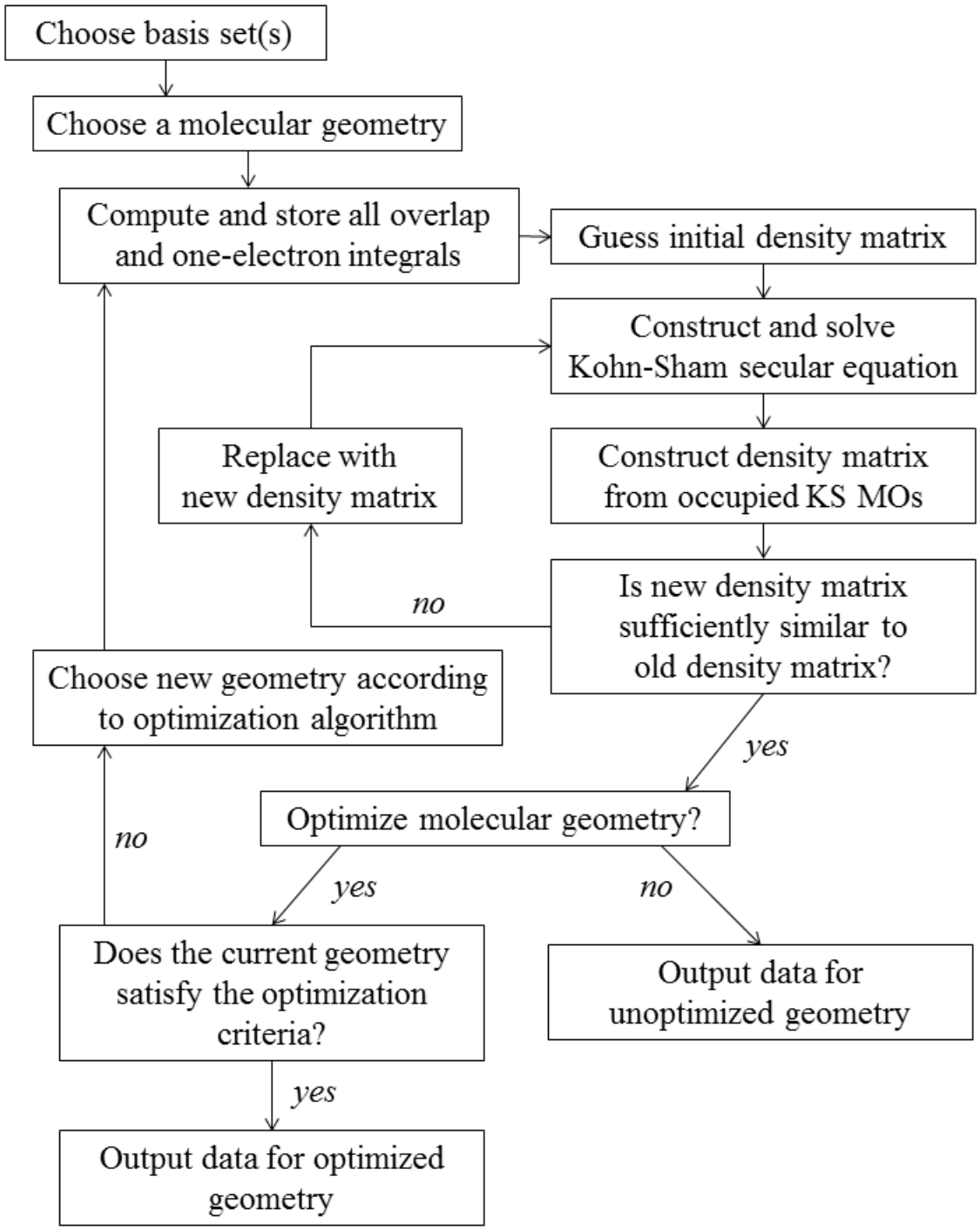

Figure 1.1 Flow chart of the Kohn-Sham SCF procedure [1].

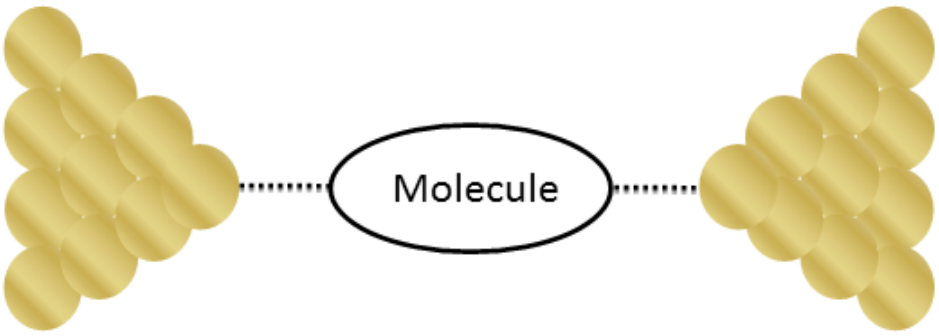

Figure 1.2 Schematic of the single molecule junction.

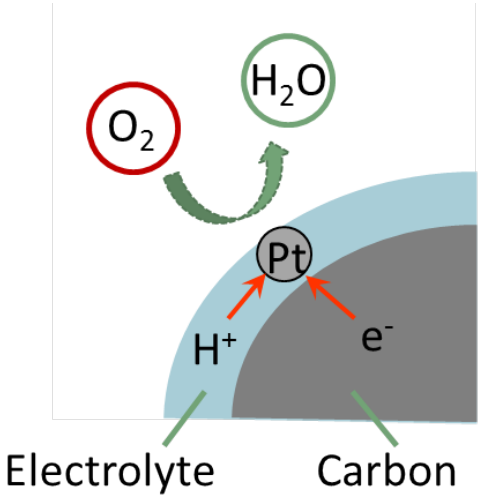

Figure 1.3 Schematic of oxygen reduction reaction on platinum with carbon support material.

References

[1] C. J. Cramer. *Essentials of Computational Chemistry : Theories and Models*. 2nd. Wiley–VCH, Inc., 2004.

[2] P. Hohenberg and W. Kohn. "Inhomogeneous Electron Gas". In: *Physical Review* 136.38 (1964), B864–B871.

[3] W. Kohn and L.J. Sham. "Self-consistent Equations including Exchange and Correlation Effects". In: *Physical Review* 140.4A (1965), A1133–A1138.

[4] T. Jacob and W. Goddard. "Water Formation on Pt and Pt-based Alloys: a Theoretical Description of a Catalytic Reaction". In: *Chemphyschem* 7.5 (2006), pp. 992–1005.

[5] P. Szarek et al. "Theoretical Study on Physicochemical Aspects of a Single Molecular Junction: Application to the Bases of ssDNA". In: *Journal of Physical Chemistry B* 117 (2013), pp. 10809–10817.

[6] S.V. Aradhya and L. Venkataraman. "Single-Molecule Junctions beyond Electronic Transport". In: *Nature Nanotechnology* 8 (2013), pp. 399–410.

[7] M.L. Perrin et al. "Large Tunable Image-charge Effects in Single-molecule Junctions". In: *Nature Nanotechnology* 8 (2013), pp. 282–287.

[8] P.A. Derosa and J.M. Seminario. “Electron Transport through Single Molecules: Scattering Treatment Using Density Functional and Green Function Theories”. In: *Journal of Physical Chemistry B* 105.2 (2001), pp. 471–481.

[9] M. Brandbyge et al. “Density-functional Method for Nonequilibrium Electron Transport”. In: *Physical Review B* 65 (2002), pp. 165401–1–16.

[10] P. Darancet et al. “Quantitative Current–Voltage Characteristics in Molecular Junctions from First Principles”. In: *Nature Letters* 12 (2012), pp. 6250–6254.

[11] D.O. Ortiz and J.M. Seminario. “Direct Approach for the Electron Transport through Molecules”. In: *Journal of Chemical Physics* 127 (2007), pp. 111106–1–3.

[12] N. Ramos-Berdullas and M. Mandado. “Revisiting the Calculation of I/V Profiles in Molecular Junctions Using the Uncertainty Principle”. In: *Journal of Physical Chemistry A* 118 (2014), pp. 3827–3834.

[13] A.J. Bard and L.R. Faulkner. *Electrochemical Methods : Fundamentals and Applications*. 2nd ed. Wiley–VCH, Inc., 2000.

[14] A. Groß. *Theoretical Surface Science: A Microscopic Perspective*. Springer Berlin Heidelberg., 2009.

Chapter 2

Details of Computational Development

2.1 Electron Transport through the Molecular Junction

Basically, the metal–molecule–metal junction causes a beneficial conductance measurement via charge transport though a weak coupling under low bias voltages. This charge transport can be explained by tunneling effect in the view point of quantum consideration and hopping mechanism in conventional scheme. The occurrence of these two mechanisms depends on the quantity of thermal phonons which grow in higher temperature and the distance of gap. Particularly, the tunneling current exponentially increases with decreasing the gap and the hopping transport is proportional to the distance [1]. As a quantum, although electrons which do not have enough energy cannot usually pass through the potential barrier, the tunneling mechanism possibly occurs when the electrons obtain the effective energy from interacting with the environment. Then, the electrons can tunnel through the molecular junction when a single molecule

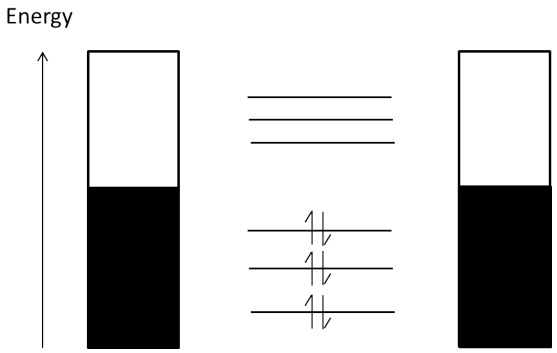

Figure 2.1 Conceptual diagram of the molecular orbital alignment in the junction.

is weakly adsorbed on the metal electrodes by overlapping their wave functions. This single molecule acts as the island between two electrodes, hence one metal which acts as a source electrode pays electron to other side which imitates a drain electrode via the molecular island [2]. On the other hand, the electron can transport by having the hopping mobility at the metal–molecule junction which has strong coupling due to the electron scattering with intermolecular vibrations [3].

As stated above, the tunneling current is principally related to the molecular orbital. The orbital energy levels of molecule are discretized and meanwhile, that of metal is almost continuous as schematically shown in Fig 2.1. Charges will flow through the metal–molecule–metal junction until the Fermi level is stabilized in a gap of the highest occupied molecular orbital (HOMO) and the lowest unoccupied orbital (LUMO) [4]. Electrons at occupied levels move to the neighboring atom from the higher chemical potential to the lower one. Concurrently, the orbitals of single molecule act as the channel of the tunneling electron. As stated in Landauer theory, the conductance of electron transmission is quantized by $G_0 = 2e^2/h$.

Inspired by an importance of molecular electronics, electronic properties of a single-molecule junction, e.g., conductance, interactions of a single-molecule with metallic electrodes, and interference effects, have been studied by both experimental and

theoretical approaches [1, 5]. Pedro et al. [6] introduced a procedure using both DFT and Green's function to examine the electron transport information through single molecules in the middle of two gold clusters . They stated the conductance in the relation to the molecular orbital and transmission function. The *I-V* characteristics were provided for different basic electronic structure. Later a well-known approach by Brandbyge et al. [7] was proposed to apply in more complicated system. Deriving from non-equilibrium Green's function formalism and the scattering states, they evaluated the current as the function of voltage and efficiently use in applications, i.e., single atom gold wires which presented the effect of finite bias result. The physical properties, which are transmission coefficient and force acting on atoms, were explained sufficiently, however, the deeply understanding of electrons movement is still indistinctive. Since, this model consisted of several computations, consequent on computational time-consuming, simpler calculation need to be improved. In addition, the obvious influence of molecular orbitals on charge transportation should be use in computation directly.

A direct *ab initio* approach [8] based on uncertainty principle was suggested. Without any empirical hypothesis, the *I-V* characteristics showed the same behavior as that of experiment. Due to its simplicity, this fundamental implementation can be developed conveniently and adopted to various arrangements of the molecule which were reported as a obstacle in experiment. Our work [9] under this consideration was also evaluated with the assumption of the transmission of charge similar to the inductive effect. Results illustrated reliable computational conductance in agreement with realistic measurement. Furthermore, a recent computation [10], that included the deformation of wave function and polarized state, was improved alternatively.

In detail, tunneling transmission in which charges travel from an atom to the other, it is known as the inductive effect in organic molecules [11]. The inductive effect describes the charge transfer along a chain of atoms in a molecule due to the

(a) (b)

Figure 2.2 (a)Charge distribution of the water molecule (blue : negative region and red : positive region) and (b) the magnitude of partial charges on each atom.

polarization in chemical bonds, for example, if an atom of high electronegativity makes a bond with others of low electronegativity, electrons are induced to move in the direction of higher attraction. Consequently, in an equilibrium condition, electrons tend to concentrate on high electronegative atoms. Thus, molecules composed of various species are usually polarized and electronegative sites have more negatively charged distributions than the others. As demonstrated in the charge distribution of a water molecule (Fig. 2.2 (a)), electrons concentrate on the oxygen atoms which has higher electronegativity than hydrogen (Fig. 2.2 (b)). The direction and magnitude of polarization is defined by the net amount of dipole moments, as sampled in Fig. 2.3. In addition, an equilibrium condition is broken when external electric fields are applied, and the behavior of electrons is affected by the fields. In an open system of single-molecule junction with a finite current density, charges will conduct through current paths generated by the polarization of molecule. In such a case, the inductive effect is suspect to have a significant role in the electrical conductivity. Similarly, in the case of tunneling current, charge transmission is expected to show high conductivity in highly polarized molecules.

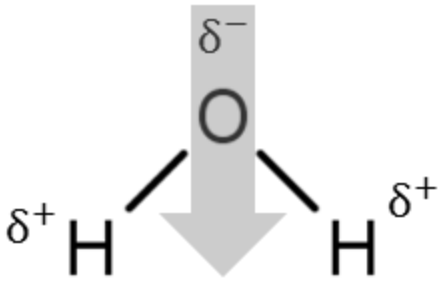

Figure 2.3 A diagram of the partial charges on the atoms and the direction of the dipole moment in a water molecule.

2.2 Descriptions of Theoretical Model

The main purpose of the present model is to explain the mechanism of charge transport through the molecular junction and to predict the unique electronic properties, i.e., I–V characteristics. There is another similar simple model with interesting procedures coupling with *ab initio* methods from a viewpoint of quantum mechanics [8, 10], however the major unique points are to compute the charge transfer and energy change.

2.2.1 Tunneling Current Computation

A particle occasionally passes through potential barriers nevertheless does not have a sufficient energy to get rid of it. This situation cannot be predicted by simple mechanics of mass points. Quantum mechanics states that a particle, which may interact and resonate with surroundings as a wave function, has the possibility to penetrate the barrier. Such a phenomenon is known as the tunneling effect. Thus, the tunneling current and the energy change via single-molecule junctions can be rationally described by the quantum mechanics. In order to compute the I–V characteristics of single molecules, tunneling current is analyzed on the basis of Heisenberg's time-energy

uncertainty principle such that

$$\Delta E \Delta t \geq \frac{\hbar}{2} \tag{2.1}$$

and the definition of electric charge current as

$$I = \frac{\Delta Q}{\Delta t} \tag{2.2}$$

Substituting Eq. (2.2) into Eq. (2.1), the electric current satisfies an inequality

$$I \leq \frac{2\Delta Q \Delta E}{\hbar} \tag{2.3}$$

where ΔE is the change of total energy that takes place in a time, Δt and I is the electric current. ΔQ is the charge transferring through the single-molecule junction, such that

$$\Delta Q = e\Delta N \tag{2.4}$$

where e is the elementary charge (1.602×10^{-19} C) and ΔN is the effective number of valence electrons involved in transmission. ΔN can be numerically analyzed by the ionization potential, IP, which describes an energy for withdrawing an electron from the molecule and the electron affinity, EA, which is the energy for adding an electron to the molecule. Concerning the applied electric field, the overall energy change per particle can be evaluated from ΔIP and ΔEA, which is the difference of the energy applying external potentials and that of neutral condition. In addition, this energy cannot exceed the energy gap of molecular orbital by the difference between the highest occupied molecular orbital (HOMO) and the lowest unoccupied molecular

orbital (LUMO), otherwise the redox reaction might occur. This HOMO–LUMO gap can be derived to the IP and EA accroding to Koopman's thorem which states that the negative value of energy level of HOMO, E_{HOMO} is equal to IP and the negative value of that of LUMO, E_{LUMO}, is equal to EA such that

$$IP = E(N-1) - E(N) = -E_{\mathrm{HOMO}} \tag{2.5}$$

$$EA = E(N) - E(N+1) = -E_{\mathrm{LUMO}} \tag{2.6}$$

where $E(N)$ is the total energy of N electron system. Hence, ΔN can be derived as follows:

$$\begin{aligned} \Delta N &= \frac{1}{2}[\frac{IP - IP_0}{2} + \frac{EA - EA_0}{2}], \\ &= \frac{1}{4}\frac{\Delta IP + \Delta EA}{IP_{\mathrm{av}} - EA_{\mathrm{av}}} \end{aligned} \tag{2.7}$$

where IP_0 and EA_0 are the ionization potential and the electron affinity of neutral system, respectively. IP_{av} and EA_{av} represent average value of the system with and without applied electric field.

In addition, one can evaluate relating electronic properties such as chemical potential, μ, and chemical hardness, η, in terms of the molecular orbital theory using the E_{HOMO} and E_{LUMO}, as simply illustrated in Fig. 2.4:

$$\mu = -\frac{E_{\mathrm{HOMO}} + E_{\mathrm{LUMO}}}{2} \tag{2.8}$$

$$\eta = \frac{E_{\mathrm{LUMO}} - E_{\mathrm{HOMO}}}{2} \tag{2.9}$$

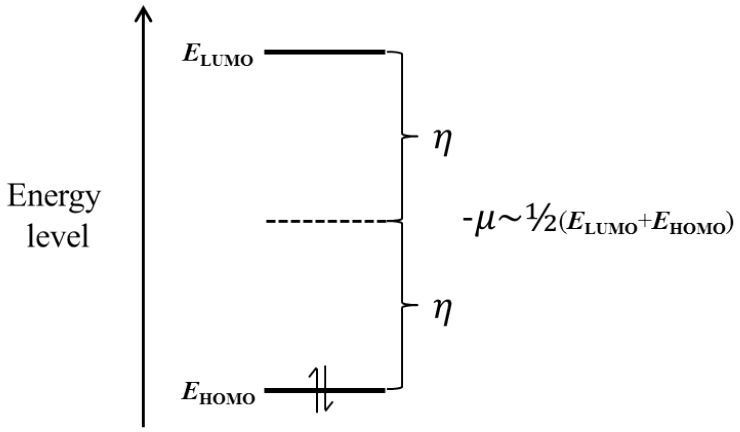

Figure 2.4 Chemical potential and chemical hardness from a molecular orbital point of view [12].

To express ΔN in a familiar way with respect to charge transfer phenomena in molecule, Eq. 2.7 was derived in term of μ and η in the ground state as shown with subscript 0, and under applied electric fields with subscript E:

$$\Delta N = \frac{1}{2}\frac{\mu_E - \mu_0}{\eta_E + \eta_0} = \frac{\Delta\mu}{2\Sigma\eta} \tag{2.10}$$

when $\Delta\mu$ represents the difference of electrochemical potential of the molecule in external potential, μ_E, and in the ground state, μ_0, and $\Sigma\eta$ is the equivalent resistance associated with the instantaneous charge generated in the molecule due to external potentials.

In detail, the definitions of the chemical potential and chemical hardness are the first and second derivative of the energy with respect to the number of electrons, respectively:

$$\mu = \frac{\partial E}{\partial N} \tag{2.11}$$

$$\eta = \frac{\partial^2 E}{\partial N^2} \tag{2.12}$$

As stated in previous section that the electron conduction is treated as a propagation of inductive effect, hence, ΔE in Eq. (2.3) is principally dominated by the polarization energy. Thus, ΔE is approximately equivalent to the inner product of induced molecular dipole moment, $\Delta\vec{D}_{\mathrm{E}}$, and the electric field, $\vec{E}$:

$$\Delta E = -\Delta\vec{D}_{\mathrm{E}} \cdot \vec{E} \tag{2.13}$$

2.2.2 Voltage Drop in Molecular Junction

A single electron transistor, in which a single molecule is placed between a pair of electrodes, shows low self-capacitance in the external electric fields at variable electric potentials. An electric potential of molecule is analyzed taking into account an assumption of the effect of charge transmission from an atom to the other one in a molecule due to the electrostatic induction that is similar to the propagation of inductive effect in organic systems [11, 13]. Since, free electrons which travel through any atoms must propagate via the nearest neighbors, the voltage drop, ΔV, across a pair of electrodes is caused by the atoms attached to the electrode surface, therefore, it is expressed as follows:

$$\Delta V = [V_{\mathrm{E}}(\vec{R}_{\mathrm{A}}) - V_0(\vec{R}_{\mathrm{A}})] - [V_{\mathrm{E}}(\vec{R}_{\mathrm{B}}) - V_0(\vec{R}_{\mathrm{B}})] \tag{2.14}$$

where A and B represent atoms at both edges of the molecule. The voltage drop is a potential difference in the external electric field, V_E, and equilibrium ground state, V_0, of atoms at $\vec{R}_A$ and $\vec{R}_B$. The potential of atom is computed by quantum mechanical

expectation value as [14],

$$V(\vec{R}_{\mathrm{A}}) = \sum_{k \neq \mathrm{A}} \frac{Z_k}{|\vec{R}_A - \vec{R}_k|} - \sum_{ij} P_{ij} \int \frac{\phi_i(\vec{r})\phi_j(\vec{r})}{|\vec{R}_{\mathrm{A}} - \vec{r}|} d\vec{r} \tag{2.15}$$

where Z_k is the atomic number of the kth atom, ϕ_i and ϕ_j are the orbital functions of the ith and jth level, respectively, and P_{ij} is a corresponding element of density matrix. This voltage drop due to the biased electric potential across the edge of the molecule in a uniform electric field can be defined clearly by using 2.14 and 2.15 as confirmed by the result of an example molecule, 4,4'-bipyridine, attached to the couple of electrodes in Fig. 2.5.

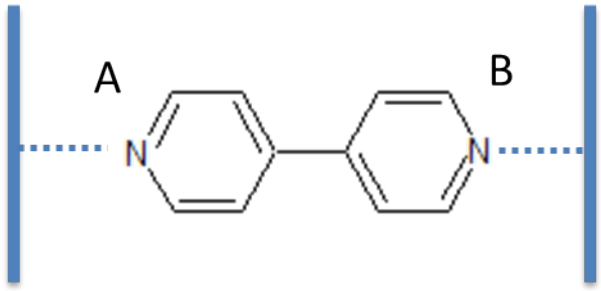

(a)

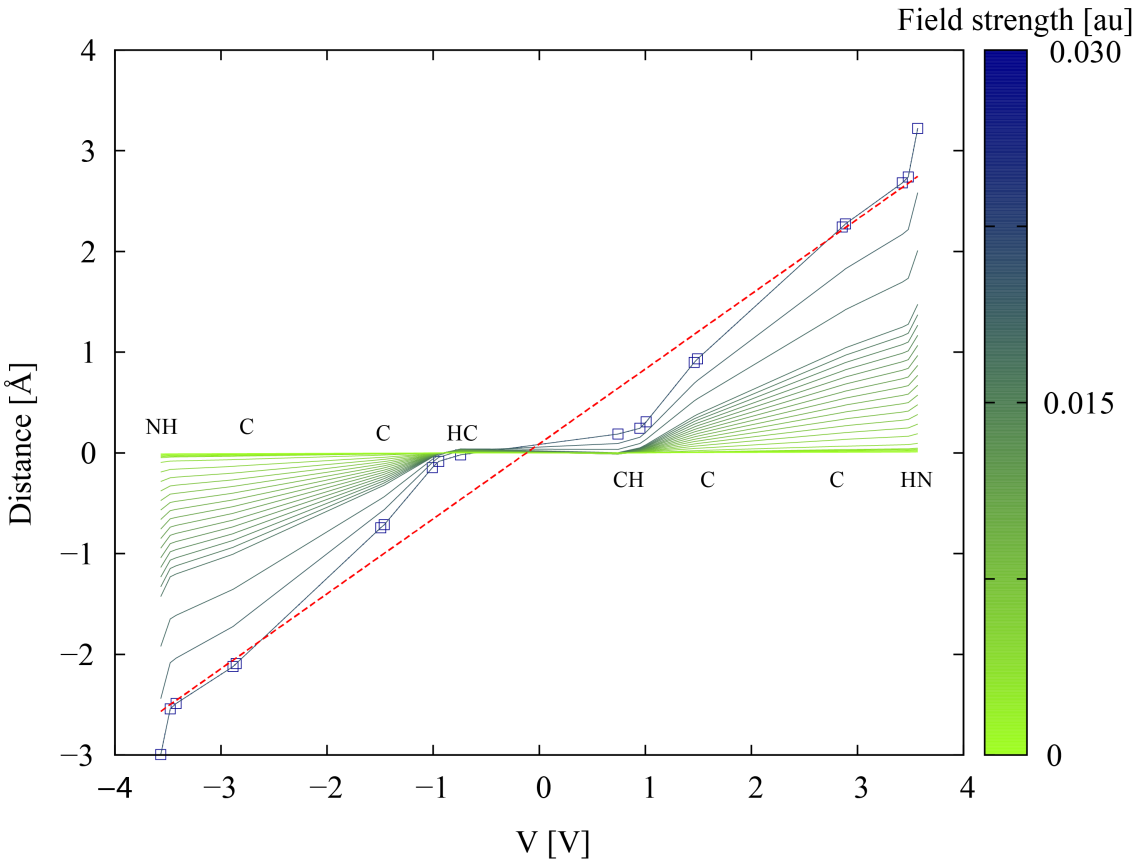

(b)

Figure 2.5 (a) Schemetic of a 4,4'-bipyridine molecule coupling with electrodes, (b) potential drop on atoms across the molecule as shown in (a) with respect to the variation of uniform electric field. Red dotted line shows the linear least squares fit of the potential drop for the largest field.

References

[1] N. A. Zimbovskaya and M.R. Pederson. "Electron Transport through Molecular Junctions". In: *Physics Reports* 509 (2011), pp. 1–87.

[2] K. Stokbro. "First-Principles Modeling of Molecular Single-Electron Transistors". In: *Journal of Physical Chemistry C* 114 (2010), pp. 20461–20465.

[3] Z. Shuai, L. Wang, and C. Song. *Theory of Charge Transport in Carbon Electronic Materials*. Springer-Verlag Berlin Heidelberg, 2012.

[4] A. Nitzan and M.A. Ratner. "Electron Transport in Molecular Wire Junctions". In: *SCIENCE* 300 (2003), pp. 1384–1389.

[5] S.V. Aradhya and L. Venkataraman. "Single-Molecule Junctions beyond Electronic Transport". In: *Nature Nanotechnology* 8 (2013), pp. 399–410.

[6] P.A. Derosa and J.M. Seminario. "Electron Transport through Single Molecules: Scattering Treatment Using Density Functional and Green Function Theories". In: *Journal of Physical Chemistry B* 105.2 (2001), pp. 471–481.

[7] M. Brandbyge et al. "Density-functional Method for Nonequilibrium Electron Transport". In: *Physical Review B* 65 (2002), pp. 165401–1–16.

[8] D.O. Ortiz and J.M. Seminario. "Direct Approach for the Electron Transport through Molecules". In: *Journal of Chemical Physics* 127 (2007), pp. 111106–1–3.

[9] P. Szarek et al. “Theoretical Study on Physicochemical Aspects of a Single Molecular Junction: Application to the Bases of ssDNA”. In: *Journal of Physical Chemistry B* 117 (2013), pp. 10809–10817.

[10] N. Ramos-Berdullas and M. Mandado. “Revisiting the Calculation of I/V Profiles in Molecular Junctions Using the Uncertainty Principle”. In: *Journal of Physical Chemistry A* 118 (2014), pp. 3827–3834.

[11] A. P. Smith, A. E. McKercher, and R. C. Mawhinney. “Inductive Effect: A Quantum Theory of Atoms in Molecules Perspective”. In: *Journal of Physical Chemistry A* 115 (2011), pp. 12544–12554.

[12] Ralph G. Pearson. “Absolute Electronegativity and Hardness Correlated with Molecular Orbital Theory”. In: *Proceedings of the National Academy of Sciences* 83 (1986), pp. 8440–8441.

[13] K. Doi, Y. Nishioka, and S. Kawano. “Theoretical Study of Electric Current in DNA Base Molecules Trapped between Nanogap Electrodes”. In: *Computational and Theoretical Chemistry* 999 (2012), pp. 203–214.

[14] B. G. Johnson, P. M. W. Gill, and J. A. Pople. “Computing Molecular Electrostatic Potentials with the PRISM Algorithm”. In: *JChemical Physics Letters* 206 (1993), pp. 239–246.

Chapter 3

Analysis of ssDNA Base Molecules by *I-V* Characteristics

3.1 Introduction

Since deoxyribonucleic acid (DNA) sequencing has valuable information to distribute the knowledge about biology and organism of humans, DNA sequencing technologies have attracted much attention in various research fields from optical techniques to electrical detection [1]. Among these fields, one of suggested sequencing methods has been relied on nanopores and nano-gapped sensing electrodes to distinguish some electrical signals between four types of nucleotides, i.e., guanine (G), adenine (A), thymine (T), and cytosine (C). Due to charges in DNA, the strand of nucleotides can be stretched through a nanopore by the strong electric field in it. In the accomplished measurement [2, 3], charge transport across single-stranded DNA (ssDNA) conducted in the direction perpendicular to the phosphate backbone which is stretched along the pore axis as presented in Fig 3.1

By this measurement, electric-current and ionic-current detection have been reported as one of the most effective methods to improve the base sequencing technique due to

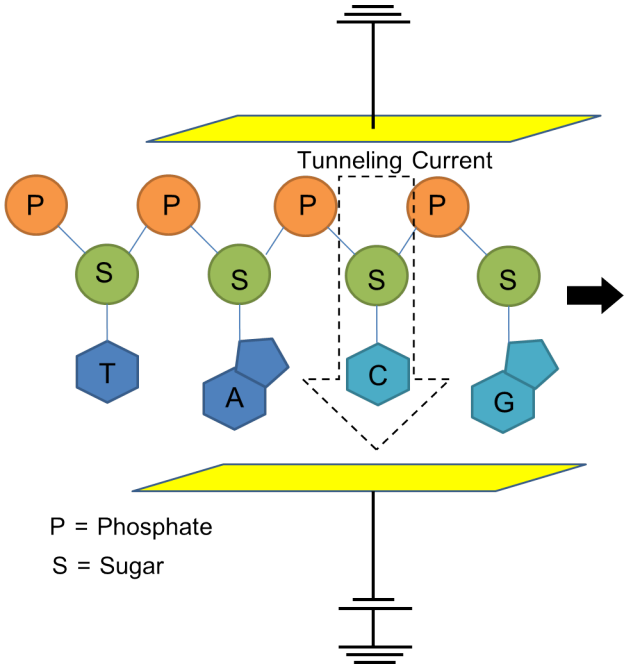

Figure 3.1 Schematic illustrations of ssDNA sequencing using nano-gapped sensing electrodes.

applying high-speed detection techniques and well-controlled flow dynamics of ions in aqueous solution [1]. In the case of ionic current measurement, one can observe ionic current blockade or conductance changes when a molecule passes through the nanopore, since the cross-section decreases due to the molecular translocation. This principle is known as Coulter-counter [4, 5]. On the other hand, electrical characteristics of DNA base sequences can be distinguished by measuring transverse tunneling current which depends on the transmission probability through a molecular junction between the detected molecule and a pair of metallic electrodes [1–3, 6]. The nano-gapped sensing electrodes in a nanopore are utilized for weak coupling with a molecule, which has an advantage in maintaining the electronic structures of trapped single molecules. A signal of tunneling current is, however, relatively smaller than that from surrounding environments. In particular, electron transmission probability is affected by electronic properties, such as electric potential and molecular capacitance, which are induced by geometry changes and charge distributions. Additionally, tunneling electrons might

exchange their energies with those of vibration modes of molecules [6]. The hopping mechanism is also observed when a traveling electron is excited enough to exceed the Coulombic potential barrier. Although it has already been proven that single nucleotides of DNA can be identified by experimental approaches as well as several kinds of models were proposed [7, 8], the detailed mechanism of phenomena has not yet been clarified. Therefore, it is necessary to review these previous literature and related topics to better understand the principle of charge transfer and computational methods.

One of experimental difficulties is to detect constant signals of each base due to the deviation of geometrical arrangements of a molecule between a pair of electrodes. That is, orientations of moving molecules cannot be fixated at the same position in solution because of thermal fluctuations [9, 10]. In order to investigate and understand such molecular phenomena in a confined space, several methods, such as empirical Landauer formalism and non-equilibrium Green's function methods [7, 8], were applied to evaluate the *I*-*V* characteristics. Although these works were able to explain the charge transfer qualitatively, the recent studies stated that the tunneling process is dominated not only by the transmission probability in the Landauer theory but also by the electronic structures of single molecule [11]. There is another simple model with interesting procedures coupling with *ab initio* methods from the viewpoint of quantum mechanics without any empirical assumption, which is based on Heisenberg's uncertainty principle [12]. In this study, we develop a theoretical model in order to characterize DNA bases by *I*–*V* characteristics according to the uncertainty principle and density functional theory (DFT) [13]. Computations are carried out focusing on a relationship between the orientation of dipole moment and energy level of frontier molecular orbitals (FMOs).

3.2 Computational Details

3.2.1 Orientation of the Single Base Molecule

Since the charge transfer is mainly described by the inductive effect, the dipole moment becomes a major factor to calculate electric current. The direction and magnitude of the induced dipole moment depend on the orientation of the molecule to the electric field. The geometry of molecule attached to the electrodes is experimentally known to have a significant role in description of tunneling current [14]. In nano-gapped electrodes, ssDNA has countless arrangements due to the flexible phosphate backbone and variations of the conductance for each base group. Referring to the experimental system [3], the space between a pair of gold nanoelectrodes is estimated as less than 1 nm. Due to such a narrow gap, ssDNA may drift into the nanogap with its phosphate backbone parallel to the electrode surface as illustrated in Fig. 3.2. Focusing on base types, i.e., G, A, T, and C as shown in Fig. 3.3, we evaluate the current which identifies the species of nucleobase. The calculations are performed for optimized base molecules where the sugar–base bond, σ_{C-N}, is replaced and terminated by a hydrogen atom. The initial configuration of all bases is defined at the angle α of σ_{C-N} with the OX direction at 61.22° and the dihedral angle of -35.04° with the OY direction. At this primary geometry denoted by $\alpha = 0°$, the surface of base plane is perpendicular to the yz plane, in other word, parallel to the electric field direction as presented in Fig. 3.4. It also explains the dependence of the surface area of the orthographic projection of the base rings on the yz plane with varying the angle α.

3.2.2 Molecule-metal Interaction

The effect of the metal–molecule–metal junction on the tunneling properties of DNA bases has been investigated in the context of their electronic polarization and related

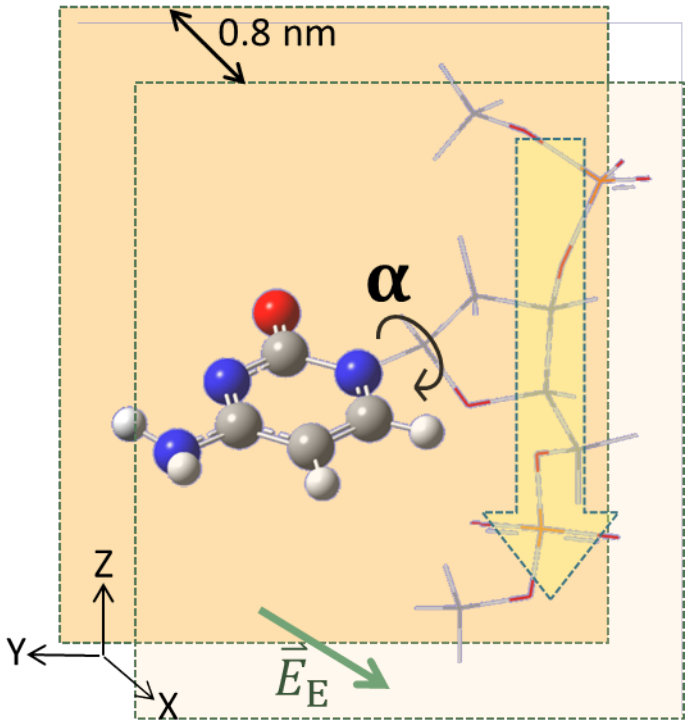

Figure 3.2 Schematic of the orientation of the ssDNA nucleobase between nano-gapped electrodes.

phenomena. As shown in Fig. 3.5, when the metal electrodes couple with the single molecule, the discrete orbital energy levels of molecule are influenced by the continuous orbital distribution of metal surface, and in addition, the orbital levels are also shifted and/or shuffled by the different applied electric voltage. Consequently, the frontier molecular orbitals corresponding to charge transport become complicated. The modulation of molecular orbital levels, induced by polarization, on the electronic transport in a molecular junction is implied. In order to investigate the effect of the molecule–metal interaction, the system including the planer gold clusters, represented by 14 atoms of Au with geometry corresponding to (111) plane, is applied. The optimized structures of gold clusters are placed parallel to each other at the position of electrode surfaces as shown in Fig. 3.6a. The isolated bases are located at the middle between a pair of clusters, where the center of mass of base and the clusters are on a line as illustrated in

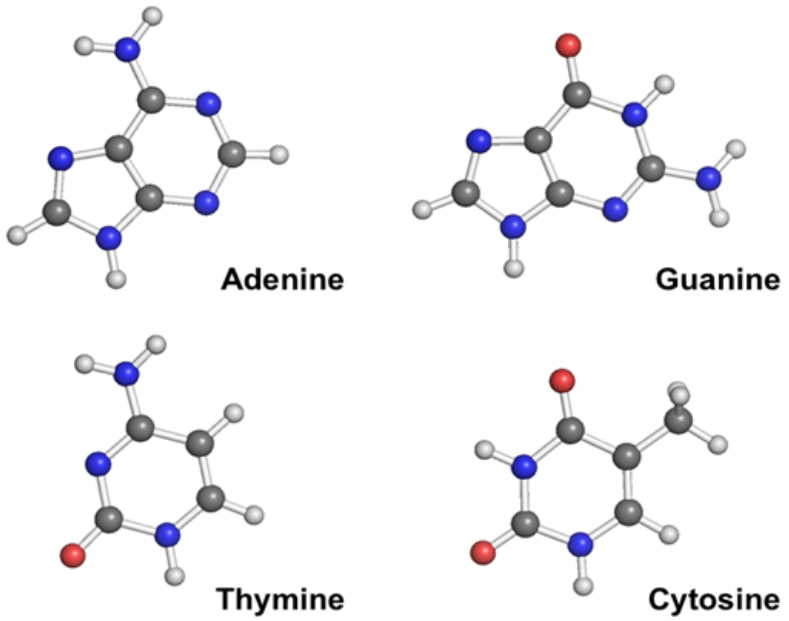

Figure 3.3 Molecular structures of isolated bases.

Fig. 3.6b. The distance between the surfaces of gold clusters is set to 0.8 nm according to the experimental set-up [3]. Furthermore, the electric field is applied in the system by a set of point charges to represent the effect of local permittivity environment on the measured current.

3.2.3 Computational Method

All calculations have been performed by using Gaussian 09 program package [15]. In the DFT methods, the Becke three-parameter hybrid functional [16] with the nonlocal correlation of Lee, Yang, and Parr (B3LYP) [17] is applied to exchange-correlation interactions, expanding the wave functions with double-ζ basis set with polarization functions by Weigend and Ahlrichs: Def2-SVP [18–20].

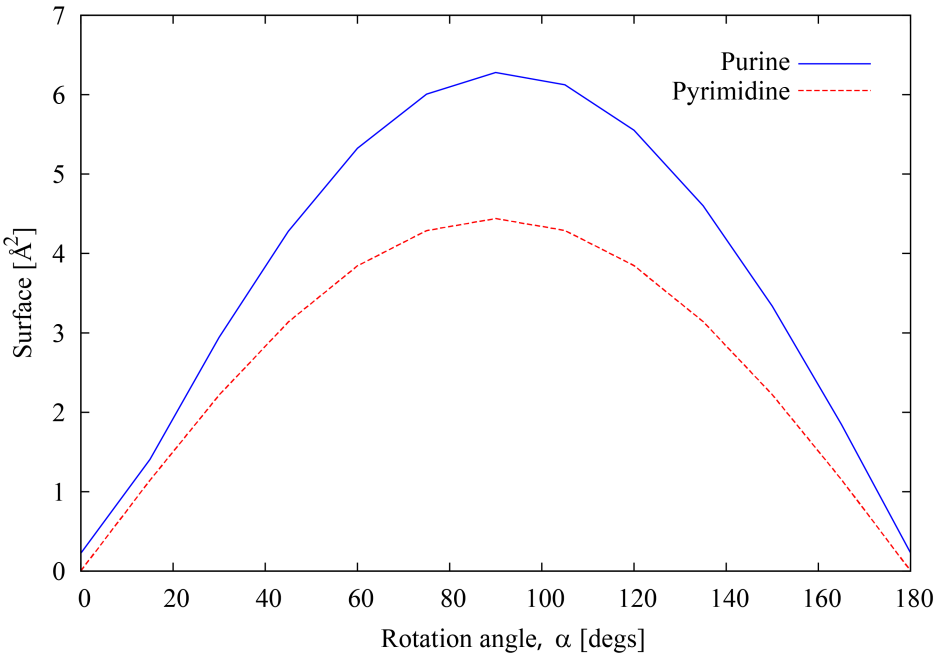

Figure 3.4 Surface area of base groups orthographically projected on the yz plane versus the rotation angle, α, for DNA.

3.3 Results and Discussion

3.3.1 *I–V* Characteristics of Base Ring Orientation

Single nucleotide measurements require identifying clear electrical signals of each individual base reducing noise. The uncertainty is caused by the freedom of base orientations, since the molecule–metal configuration is important to the charge transport. Hence, the I–V characteristics are collected for the base ring orientation in ssDNA, which rotated around a bond with sugar group by using our developed theoretical model. Note that the deoxyribose–phosphate backbone was constrained in the direction parallel to the electrode surface. Although this structure still seems to be independent, it can define the precious trend of projected surface as shown in Fig. 3.4. Moreover, since the charge transfer is mainly described by the inductive effect due to the polarization, the dipole moment becomes a major factor to calculate electric current. The direction and magnitude of induced dipole moments depend on the orientation of molecules to

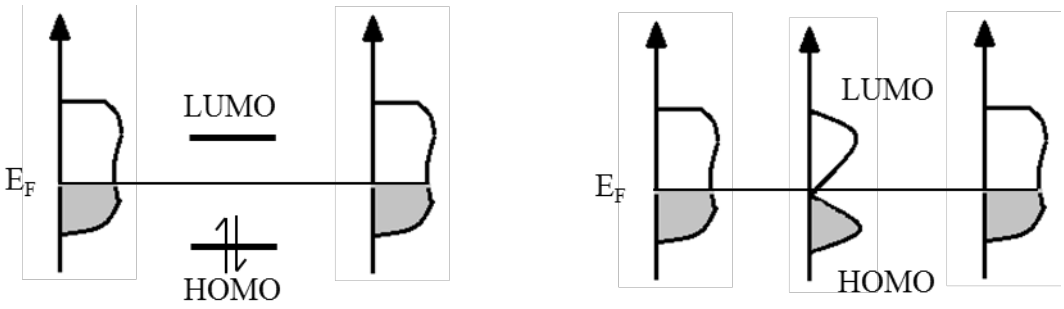

Figure 3.5 Schematic of molecular orbital change due to the molecule-metal interaction.

Table 3.1 The rotation angles which correspond to the highest current.

Base	Angles
Adenine	75°, 90°, 270°, 285°
Guanine	105°, 255°
Cytosine	75°, 285°
Guanine	90°, 270°

an external electric field. The *I–V* characteristics for 360° rotation around sugar–base bond, σ_{C-N}, with the interval of 15° are shown in Fig. 3.7. Results from A and G are more dispersed than those of C and T. The highest density of bundles are located at high current regions that correspond to the rotation angles as detailed in Table 3.1 and it can be usually observed at near α= 90° and α= 270°. This trend can also be confirmed by electron scattering simulations in a previous study, where electrons tended to be attracted by bases when they were injected perpendicular to the molecular surfaces and resulted in the high conductance [21].

In Figure 3.8, the average lines are compared between all bases. Although the results are quite similar for each base, the averaged values show a tendency of conductance as following: A and G > T and C concurrent with the experimental result [3] and theoretical ones [8, 21]. Comparing between pyrimidines, the conductance of C is greater than T when the applied voltage is below 0.4 V, on the contrary, in the range near 0.4 V, the conductance of T becomes higher than that of C. Moreover, as shown in Table 3.2, the chemical potential of purines is lower than that of pyrimidines. The

chemical potential causes a potential barrier between different species which defines the capability of electron transmission. Therefore, a molecule with a low chemical potential allows an electron to pass through easier than that with a high chemical potential. As a result, the conductance of purines (A and G) is higher than that of pyrimidines (C and T). This trend coincides with the characteristics of conductance resulting from Fig. 3.8 and other results [3, 8, 21]. From all reasons above, one can say that the electronic structures are affected by the applied electric field induce molecular dipole moment, $\Delta\vec{D}_{\mathrm{E}}$, and ΔN. That is, the polarization and electron transfer strongly depend on the external potential.

3.3.2 Analysis of electronic properties on molecule–metal interaction

In this section, computations have performed including the gold clusters to clarify the effect of interaction of metal atoms to the DNA bases such as the electronic structure rearrangement by the shifting and splitting of molecular orbital energy levels. Moreover, the effect of the local permittivity environment (LPE) [22] are considered on the measured current, thus it is imitated by using the non-uniform permittivity.

A major difficulty in computations which include electrode materials is to suitably determine E_{HOMO} and E_{LUMO} from Eqs. (2.5) to (2.7) crucial for the tunneling current calculation, since the orbital levels are composed of a base molecule and Au atoms. In order to identify each base by tunneling current, these energy levels should be mainly dominated by a base not by Au. From an experimental point of view, the tunneling current can clearly distinguish a single molecule. On the other hand, the orbital coefficients allow us to determine major components on an eigenstate. Here, in order to specify the most effective molecular orbitals of bases on the tunneling current, we analyzed and visualized the distribution of coefficients near the HOMO and LUMO.

Table 3.2 Electronic properties of DNA bases.

Base	HOMO (eV)	LUMO (eV)	Chemical potentail (eV)	Chemical hardness (eV)
Adenine	-6.031	-0.601	3.316	2.715
Guanine	-5.730	-0.218	2.974	2.756
Cytosine	-6.708	-1.178	3.943	2.765
Guanine	-6.300	-0.928	3.614	2.686

Table 3.3 Molecular orbital energy associated with the computation.

Base		Occupied state		Unoccupied state	
	dV	Orbital No.	Energy (eV)	Orbital No.	Energy (eV)
A	0.0 V	HOMO-2	-0.22374	LUMO+10	-0.07641
	0.6 V	HOMO-3	-0.22624	LUMO+10	-0.08442
G	0.0 V	HOMO-2	-0.21403	LUMO+10	-0.07880
	0.6 V	HOMO-1	-0.21554	LUMO+10	-0.08556
C	0.0 V	HOMO-4	-0.23234	LUMO+10	-0.07813
	0.6 V	HOMO-3	-0.23217	LUMO+10	-0.08629
T	0.0 V	HOMO-4	-0.24211	LUMO+10	-0.07989
	0.6 V	HOMO-4	-0.23828	LUMO+10	-0.08807

Figure 3.9 shows the fraction of the absolute sum of orbital coefficients on atoms in bases to the whole system. To calculate tunneling current, we selected molecular orbitals with regard to not only high contribution of base atoms but also the closest orbital to the HOMO and LUMO, which have a high possibility of contribution to charge transfer. To do so, we focus on molecular orbitals near the Fermi level (at x = 0 in Fig. 3.9) with the fraction over 0.2. In Table 3.3, the critical molecular orbitals in Au–base–Au junctions are listed for typical cases in equilibrium and under an electric potential of 0.6 V. Particularly, for the case of adenine junction with 14 Au clusters, the HOMO, LUMO and other occupied and unoccupied states mainly dominated by the adenine is visualized in Fig. 3.10.

As shown in Fig. 3.10a, the molecular orbitals of HOMO-2 and LUMO+10 show concentrations of the wave function on the adenine more strongly than those of the

HOMO and LUMO. Under the electric potential, as shown in Fig. 3.9, the occupied molecular orbitals remain at almost the same levels with respect to the ground state, so that to identify the transition of the occupied states is easier comparing with the unoccupied states which show more complexity. Fig. 3.10b, the symmetric distribution of electrons are broken by the applied electric potential, where the direction of electric field is from the left to right. Especially, orbitals of the HOMO-3 and LUMO+10 show drastic changes. Although these results are obtained as the ground state, we can schematically explain the polarization of electrons in the electrically biased condition. For example, it is suggested that an electron in the left Au electrode is injected in the LUMO+10 and simultaneously an electron in the HOMO-3 is extracted by the right Au electrode and that the excited state at the LUMO+10 goes down to the HOMO-3. Figure 3.11 shows the I–V characteristic of all bases with the 14 Au atoms. It shows that the conductance of purines (A and G) is higher than that of pyrimidines (C and T). The lines are more clearly different between each other when compare with the previous results in uniform electric field, as presented by dashed lines in Fig. 3.11. Moreover, the current becomes relatively smaller, which is much closer to the experimental data [3], since the potential barrier due to the nanogap and screening effect caused by electrons on the Au atoms are taken into account by the Au clusters. The tendency, however, may still not be in definite accuracy comparing with the experimental result [2, 3], since the selected molecular orbitals contributing to the current and the molecular structure of Au clusters should be more suitably optimized. To improve the selected molecular orbitals, projected density of states (PDOS) analysis by including FMO of Au atoms is considered as a promising method.

3.4 Concluding remark

The developed model could sufficiently explain the effect of molecular arrangement and I–V characteristics of ssDNA [23]. It may be available to investigate effects of molecular arrangements and vibrations in tunneling current measurement of ssDNA. The electric current relied on the molecular polarization energy and dipole moment has been analyzed with the variation of base ring orientations. The results show similar trends of the conductance as previous experimental [2] and computational [8, 21] results. In addition, the analysis on interaction between DNA base molecules and the metal clusters was also studied and the results showed a more realistic comparison with the previous results due to considering potential barriers at the interface and screening effect. However, it is supposed that further studies about the analysis of selected molecular orbital and the molecular structures of Au clusters are also required for quantitative discussions.

The present results are expected to be coupled with molecular dynamics simulation in our future work [9, 10]. In our previous work [24], the simulation of dissociative adsorption of a H_2 molecule on a steric graphene surface has already succeeded, where electron concentrations on a steric carbon site induced dissociation of a H_2 molecule and charges transferred as it approached to the surface. Applying this technique, we hope to discuss the dynamical aspect. In order to treat such large molecules, however, further technical improvements will be required.

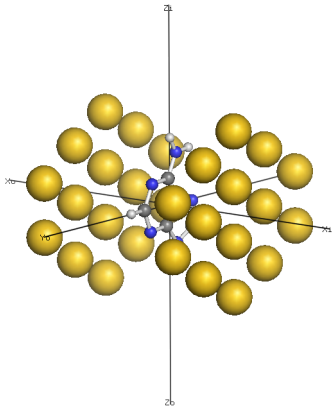

(a) Three-dimensional view

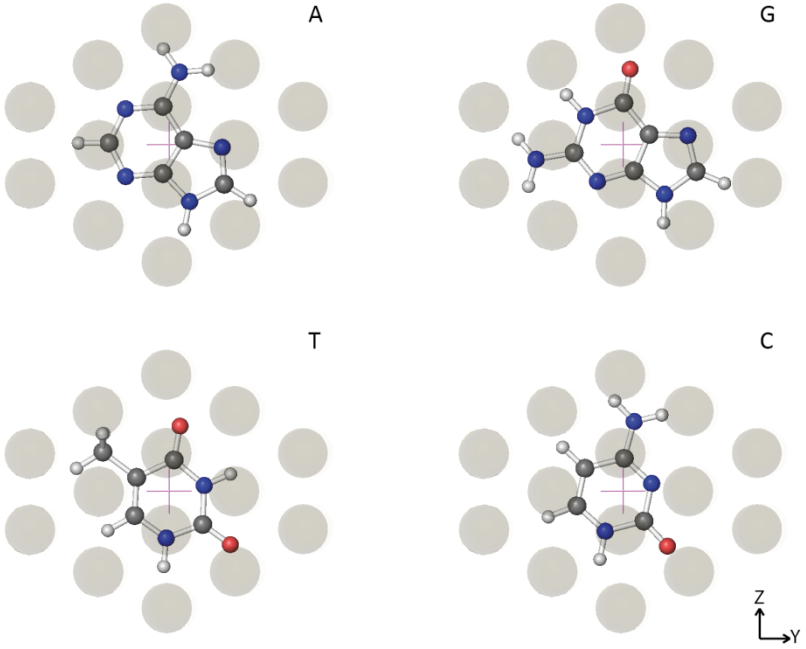

(b) Side view

Figure 3.6 Schematic of the geometry of DNA bases and Au clusters of 14 Au atoms represented by hydrogen (light gray), carbon (gray), nitrogen (blue) and oxygen (red). The symbol "+" represents the position of the center of mass of a base and individual Au clusters projected on the *yz*-plane.

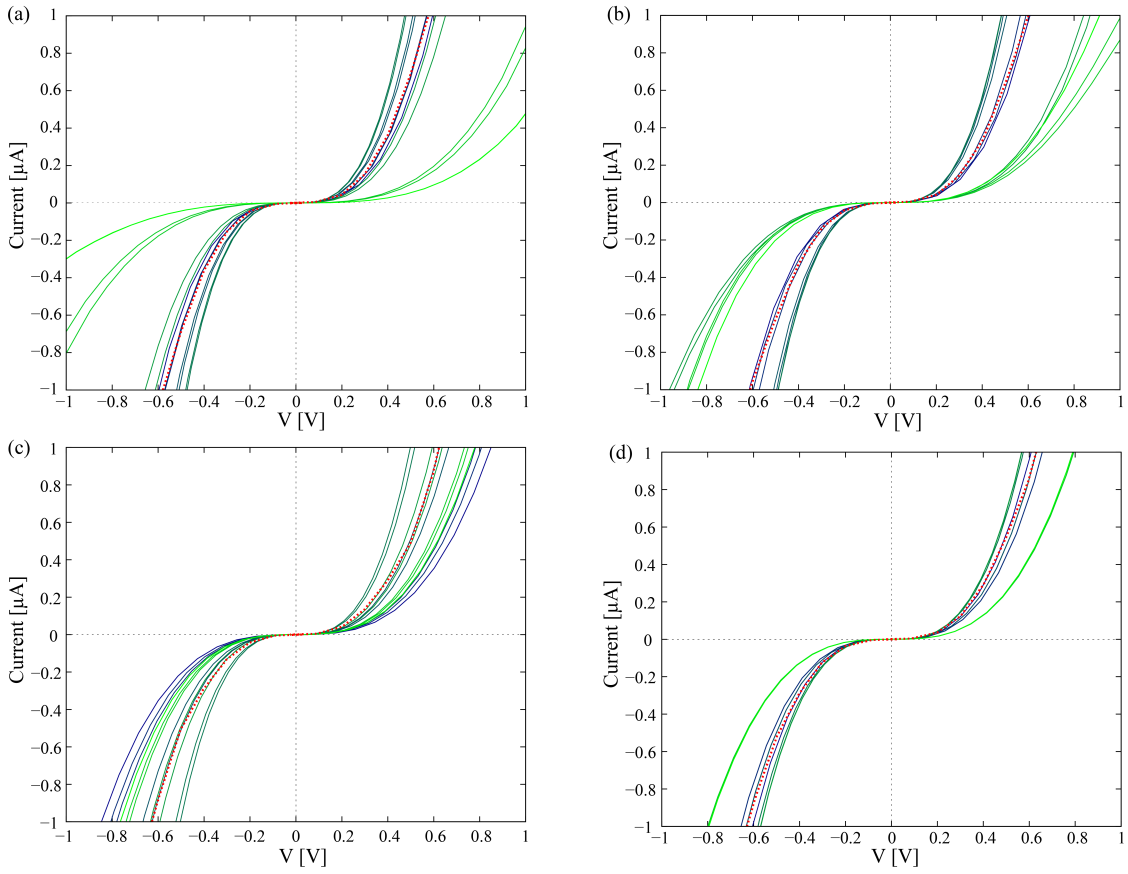

Figure 3.7 I-V characteristics for 360° rotation around σ_{C-N}: (a) adenine, (b) guanine, (c) cytosine and (d) thymine. Dotted lines (red) represent averaged characteristics.

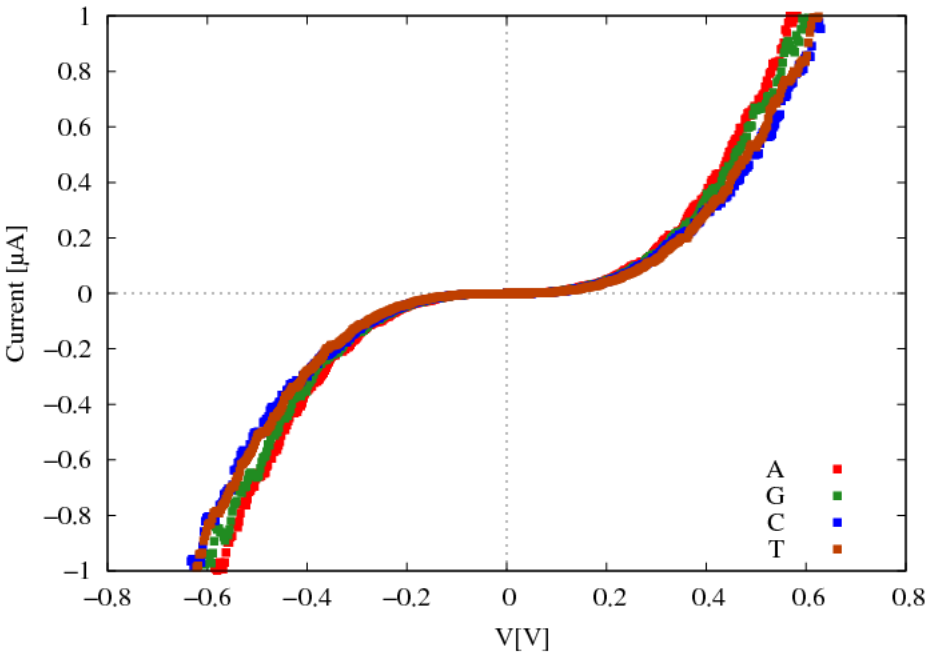

Figure 3.8 Comparison of averaged I-V characteristics for all bases.

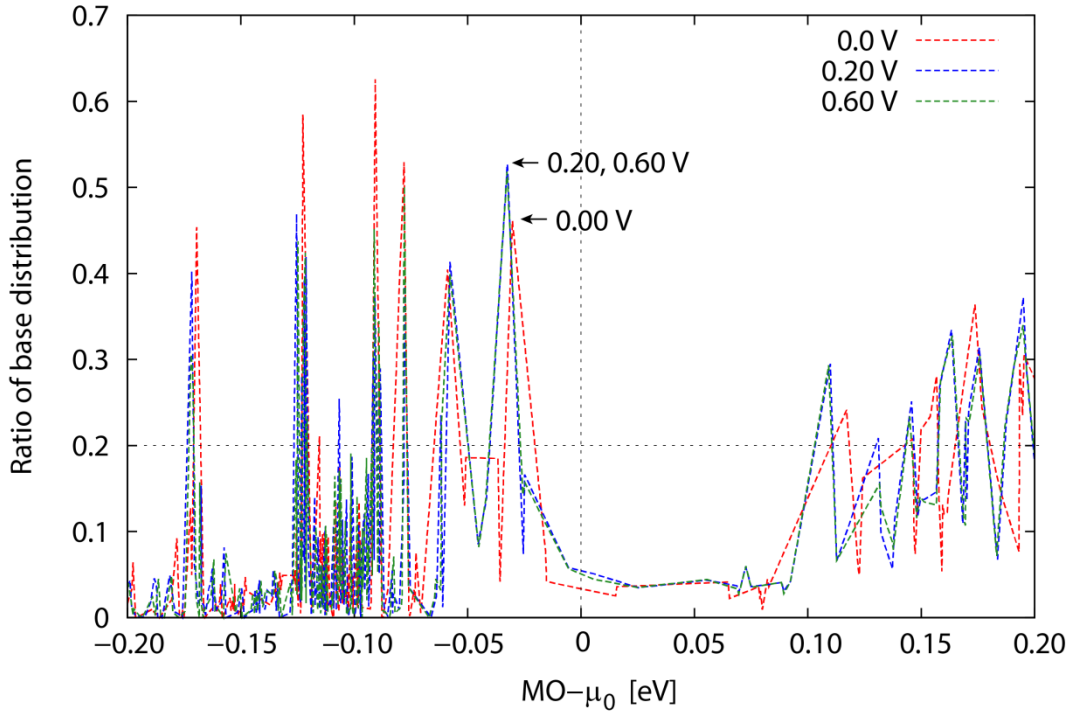

(a) Adenine

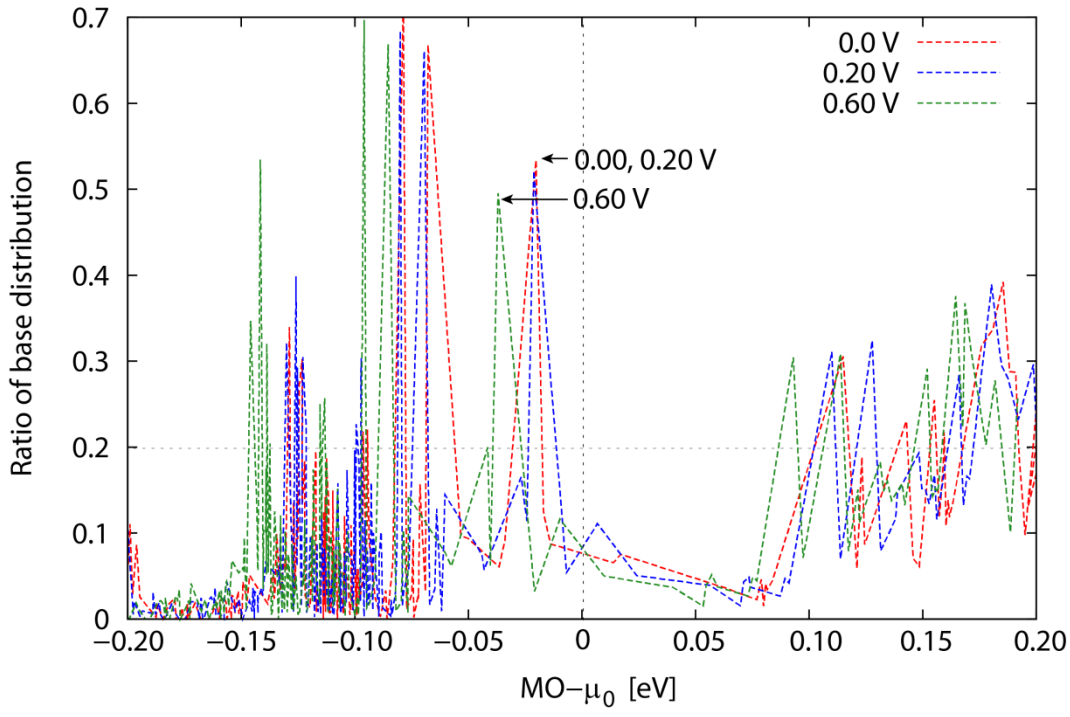

(b) Guanine

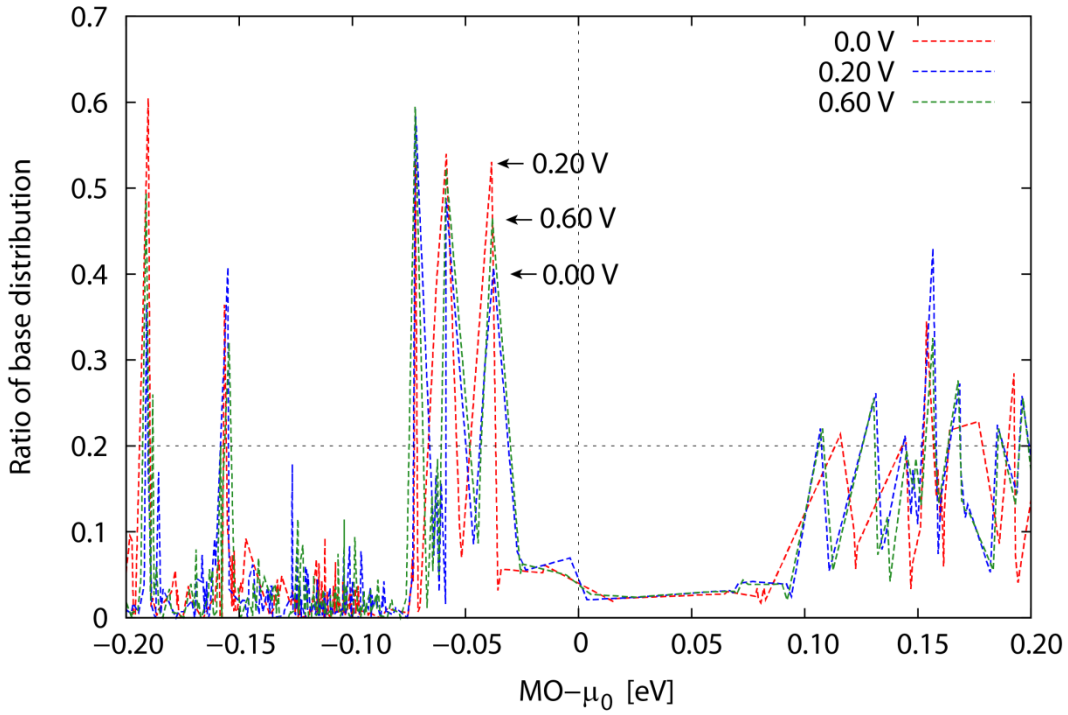

(c) Cytosine

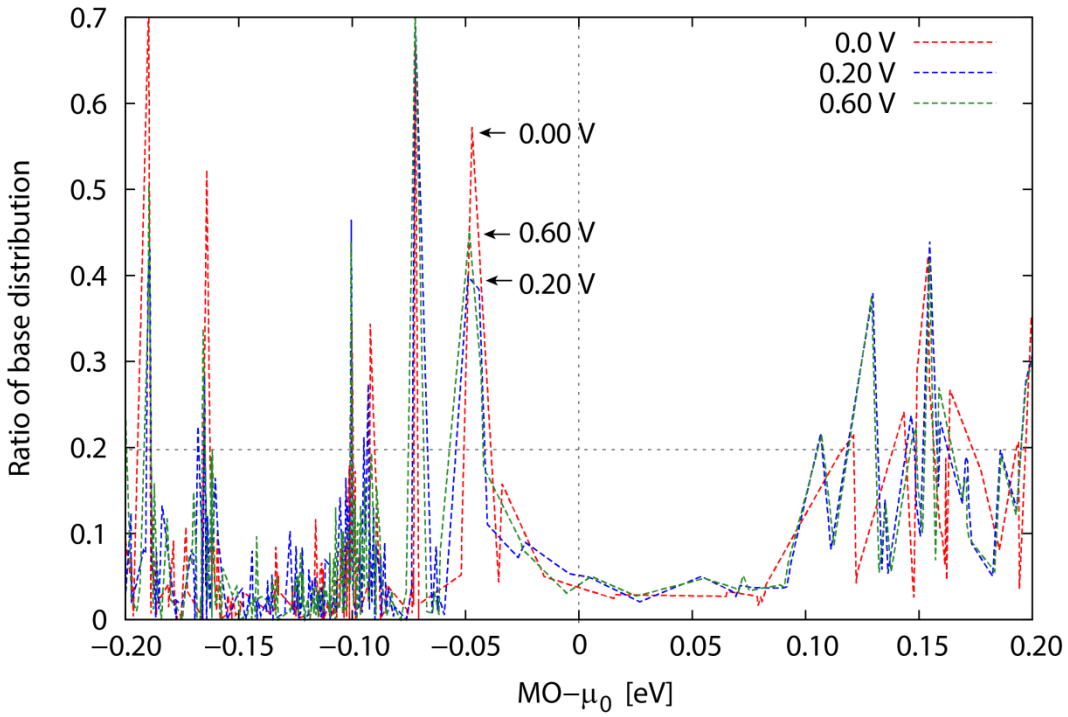

(d) Thymine

Figure 3.9 The ratio of base atom contribution to overall molecular orbitals at varied electric fields with respect to the difference of molecular orbital (MO) and chemical potential (μ_0) of the neutral system (x–axis).

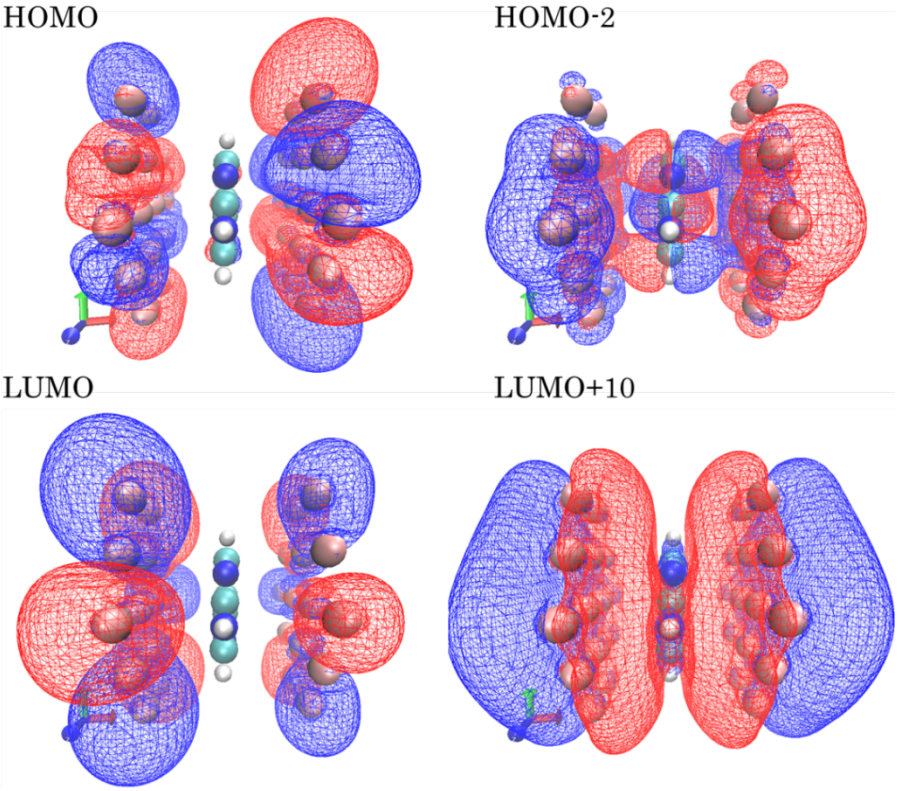

(a) Neutral system

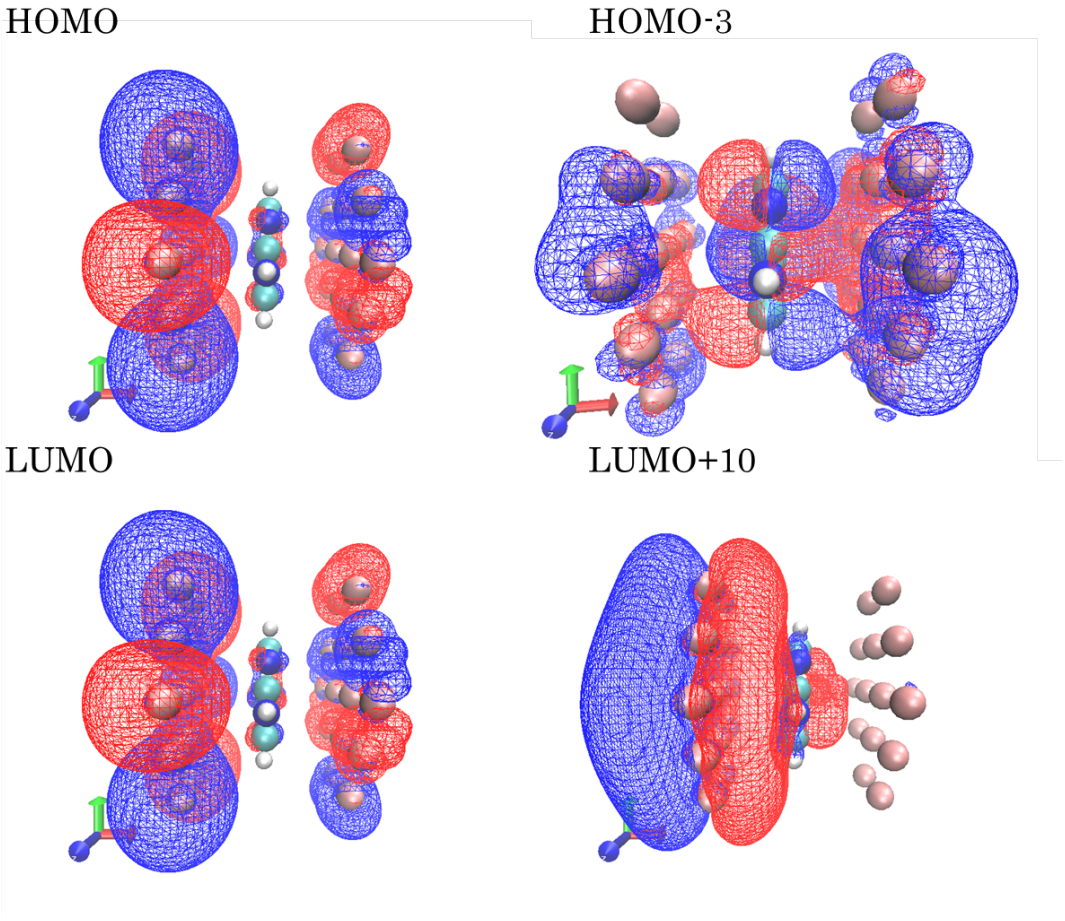

(b) Applied electric field system

Figure 3.10 Visualization of frontier molecular orbitals of adenine with clusters of 14 Au atoms: (a) neutral and (b) applied electric field system. Red (blue) regions correspond to plus (minus) sign of coefficients.

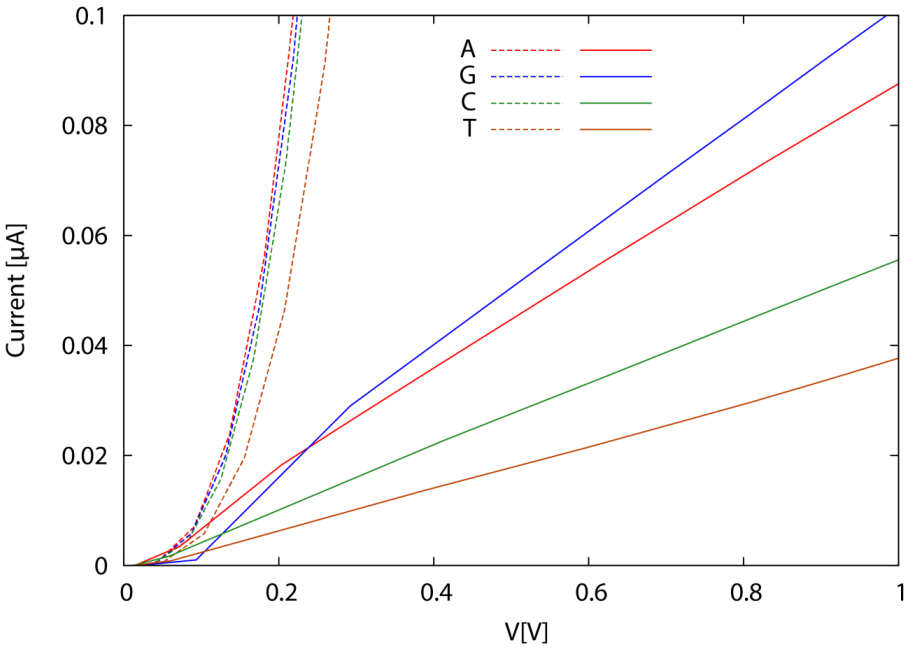

Figure 3.11 I–V characteristics of all bases with Au clusters of 14 Au atoms in non-uniform electric field (solid line) and in uniform electric field without Au clusters as shown in Fig. 3.8 (dashed line).

References

[1] M. Zwolak and M. Di Ventra. "Colloquium: Physical approaches to DNA Sequencing and Detection". In: *Reviews of Modern Physics* 80 (2008), pp. 141–165.

[2] M. Tsutsui et al. "Identifying Single Nucleotides by Tunnelling Current". In: *Nature Nanotechnology* 5 (2010), pp. 286–290.

[3] T. Ohishiro et al. "Single-Molecule Electrical Random Resequencing of DNA and RNA". In: *Nature Nanotechnology* 2.501 (2012), pp. 1–7.

[4] T.Z. Butler et al. "Single-molecule DNA detection with an Engineered MspA Protein Nanopore". In: *Proceedings of the National Academy of Sciences of the United States of America*. Vol. 105. 52. Dec. 2008, pp. 20647–20652.

[5] G.F. Schneider et al. "DNA Translocation through Graphene Nanopores". In: *Nano Letters* 10.8 (2010), pp. 3163–3167.

[6] B. Ulgut and H.D. Abruña. "Electron Transfer through Molecules and Assemblies at Electrode Surfaces". In: *Chemical Reviews* 108.7 (2008), pp. 2721–2736.

[7] M. Zwolak and M. Di Ventra. "Electronic Signature of DNA Nucleotides via Transverse Transport". In: *Nano Letters* 5.3 (2005), pp. 421–424.

[8] J. Lagerqvist, M. Zwolak, and M. Di Ventra. "Fast DNA Sequencing via Transverse Electronic Transport". In: *Nano Letters* 6.4 (2006), pp. 779–782.

[9] K. Doi et al. “Development of Coarse-Graining DNA Models for Single-nucleotide Resolution Analysis”. In: *Philosophical Transactions of the Royal Society A* 368 (2010), pp. 2615–2628.

[10] K. Doi, T. Uemura, and S. Kawano. “Molecular Dynamics Study of Solvation Effect on Diffusivity Changes of DNA Fragments”. In: *Journal of Molecular Modeling* 17 (2011), pp. 1457–1465.

[11] N. A. Zimbovskaya and M.R. Pederson. “Electron Transport through Molecular Junctions”. In: *Physics Reports* 509 (2011), pp. 1–87.

[12] D.O. Ortiz and J.M. Seminario. “Direct Approach for the Electron Transport through Molecules”. In: *Journal of Chemical Physics* 127 (2007), pp. 111106–1–3.

[13] P. Geerlings, F. De Proft, and W. Langenaeker. “Conceptual Density Functional Theory”. In: *Chemical Reviews* 103.5 (2013), pp. 1793–1873.

[14] B. Xu and N. J. Tao. “Measurement of Single-Molecule Resistance by Repeated Formation of Molecular Junctions”. In: *Science* 301 (2003), pp. 1221–1223.

[15] M. J. Frisch et al. *Gaussian09 Revision A.01.* Gaussian Inc. Wallingford CT 2009.

[16] A. D. Becke. “Density-Functional Thermochemistry. III. The Role of Exact Exchange”. In: *Journal of Chemical Physics* 98 (1993), pp. 5648–5652.

[17] C. Lee, W. Yang, and R. G. Parr. “Development of the ColleSalvetti Conelation Energy Formula into a Functional of the Electron Density”. In: *Physical Review B* 37 (1988), pp. 785–789.

[18] F. Weigend and R. Ahlrichs. “Balanced Basis Sets of Split Valence, Triple Zeta Valence and Quadruple Zeta Valence Quality for H to Rn: Design and Assessment of Accuracy”. In: *Physical Chemistry Chemical Physics* 7 (2005), pp. 3297–3305.

[19] D. Feller. “The Role of Databases in Support of Computational Chemistry Calculations”. In: *Journal of Computational Chemistry* 17 (1996), pp. 1571–1586.

[20] K. L. Schuchardt et al. “Basis Set Exchange: A Community Database for Computational Sciences”. In: *Journal of Chemical Information and Modeling* 47 (2007), pp. 1045–1052.

[21] K. Doi, Y. Nishioka, and S. Kawano. “Theoretical Study of Electric Current in DNA Base Molecules Trapped between Nanogap Electrodes”. In: *Computational and Theoretical Chemistry* 999 (2012), pp. 203–214.

[22] M. Zhang et al. “DNA Electrokinetic Translocation through a Nanopore: Local Permittivity Environment Effect”. In: *The Journal of Physical Chemistry C* 116 (2012), pp. 4973–4801.

[23] P. Szarek et al. “Theoretical Study on Physicochemical Aspects of a Single Molecular Junction: Application to the Bases of ssDNA”. In: *Journal of Physical Chemistry B* 117 (2013), pp. 10809–10817.

[24] K. Doi, I. Onishi, and S. Kawano. “Dissociative Adsorption of H_2 molecules on Steric Graphene surface: Ab Initio MD Study Based on DFT”. In: *Computational and Theoretical Chemistry* 994 (2012), pp. 55–64.

Chapter 4

Analysis of ORR near Biased Electrode Surfaces

4.1 Introduction

One of the most attractive issues in the surface science is the interaction of oxygen and metal surface since this process consists of complicated fundamental steps. Especially, the oxygen reduction reaction (ORR) on the platinum surface has been a presently interesting research owing to a major role in the fuel cells. Regarding to the highest binding energy of double bond in the oxygen molecule, the ORR is the slowest step of the whole electrochemical reactions, thus, it is the rate-determining step of overall system. Hence, the development relating to the ORR and catalyst material has to be studied [1–3].

In details, the fuel cells are the device that generates electricity via electrochemical reaction as summarized in Fig. 4.1. Their components are an anode where hydrogen oxidation reaction (HOR) occurs, an electrolyte membrane that allows the flow of proton from anode to the cathode, and a cathode in which ORR takes places. The hydrogen fuel diffuses to anode layer, simultaneously, the oxygen gas obtained from the

air disperses to cathode layer, then, hydrogen molecules are oxidized to protons (H^+) and electrons (e^-). Protons penetrate through the electrolyte layer, while electrons flow from anode to cathode via the external circuit in which electric current occurs, at last, these protons and electrons react with oxygen which dissociates and adsorbs onto catalyst molecules, i.e., platinum (Pt). As shown in Figure 4.2, the usual configuration of catalyst layer is featured with platinum particles formed on larger carbon particles that can be called carbon-supported Pt catalyst. Due to diverse objectives of practical use and operating environment, there are several types of fuel cells. Among of them, the proton exchange membrane fuel cells (PEMFCs) are attractive equipment regarding to their low operating temperature and applicability in both stationary and portable applications, especially in the vehicles. However, to apply in the commercial use, the most critical obstacles are the large overpotential and the extremely high production cost due to the rare materials in catalyst. The overpotential problem describes the potential difference between the open-circuit potential, which is an ideal value, and the practical potential. As shown in Figure 4.3, the major loss in low current density region is the kinetic losses which principally caused by the high overpotential in ORR. Moreover, some ways to reduce the production cost are increasing the catalytic activity mainly dominated by the surface reactions and introducing alternative catalyst material.

To conquer this insufficiency in catalyst, research works in 1990s to 2000s focused on the development of platinum-based catalyst in two ways, one is increasing the activity and utilization of the surface area of the platinum catalyst within the electrode and the other way is finding the alternative material such as the platinum alloy catalyst or non-metal material to reduce requirement of platinum that also causes the high cost problem. To enhance the activity per surface of catalyst, the critical point which needs to be considerably investigated is structural parameters, thus, various topics were

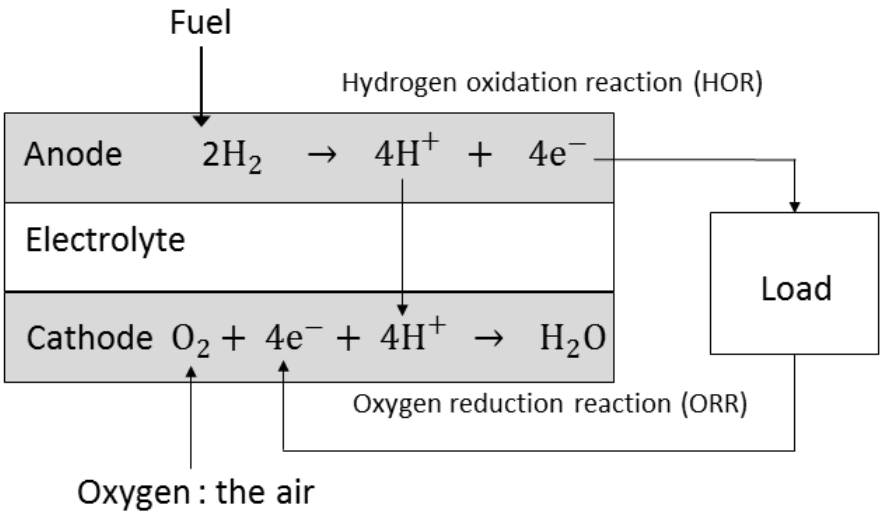

Figure 4.1 Conceptual schematic of fuel cells.

carried out in order to archive the higher efficiency such as the platinum particle size effect. Nevertheless, some works suggested that there is no effect on activity per unit mass of platinum with decreasing in the particle size, for example, the experimental result in gas phase showed that no specific difference on ORR activity with various platinum particle sizes [5, 6]. Hence, these studies required the high amount of platinum use, therefore an alternative material becomes a powerful interesting field of study, nonetheless, the electronic and chemical properties of electrode surface require high and accurate adjustment. Alternatively, studies on the substitute catalyst material initially focused on the metal alloy of platinum [7]. Moreover, the non-metal catalyst, i.e., nitrogen-doped carbon nanotube (NCNTs) has been introduced and improved to accomplish both the lower price and the higher chemical reaction rate [8]. Although these previous experimental works had examined the catalyst material efficiently, they were restricted in the working scope to investigate the atomic-level interaction.

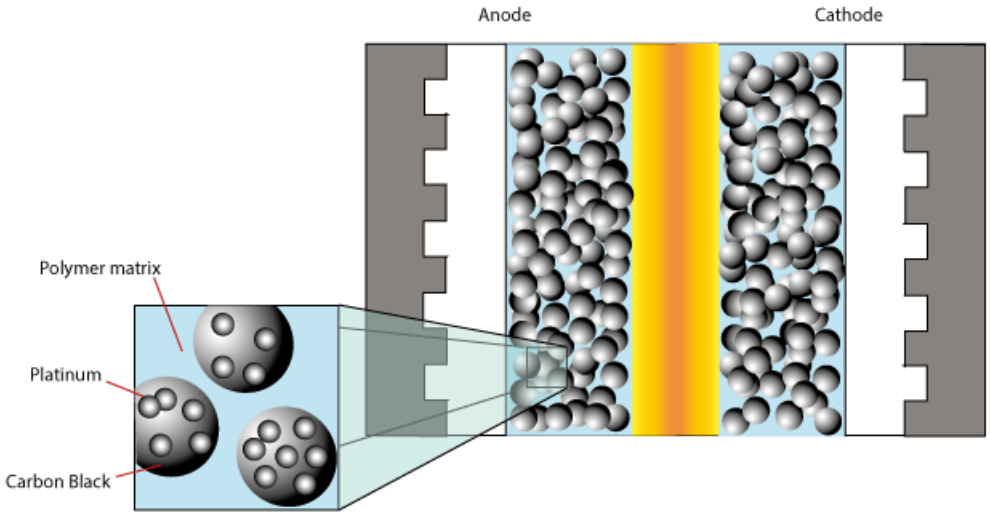

Figure 4.2 Structural schematic of fuel cells.

In the atomistic point of view, the principal interesting trends of research on ORR have been finding actual pathways which can explain the complicated mechanism and point out what is the main reason of high energy barrier. This issue has performed on the atomistic computation concurrently with experiments. The experimental works reported the ambiguous pathways in dissociative adsorption of oxygen molecule on platinum. Luntz et al. [9] observed both direct and precursor-mediated dissociative dynamics of ORR and they applied the sticking coefficient to measure the probability for dissociative chemisorption. Nevertheless, Zambelli et al. [10] used the scanning tunneling microscope (STM) to study the distribution of oxygen on the platinum(111) surface. They reported that oxygen has both physisorption and chemisorption depending on temperature and the structures of adsorbate molecule were changed during weak adsorption.

Due to consuming time and catalyst material which is difficulties in experiment, the molecular computational procedure, based on the mathematical quantum theory and/or empirical derivation, has been necessary to clarify the complication of ORR

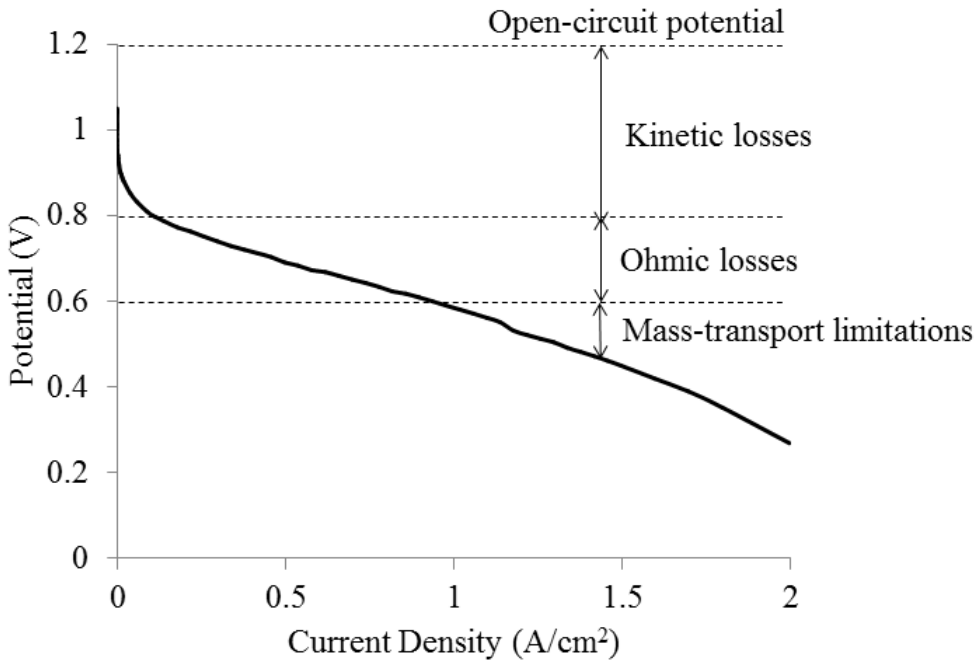

Figure 4.3 Schematic of a *I-V* characteristics showing the typical losses at high current densities [4, 5].

on platinum/carbon surface [11]. It can elucidate the interaction of particles and surface, generate the reliable electronic structure and explain the electronic behavior. There are macroscopic scale numerical calculations, which take the computational fluid dynamics into account, and the molecular level computations. This approach is normally performed to simulate the whole system of PEMFCs which consist of an anode, a cathode and a electrolyte layer, however, they are limited to explain interface problems within nanoscale [4]. Meanwhile, the molecular calculations have been taken into account of investigation of catalyst surface. Most previous molecular studies of ORR generally illustrated the results by the energy diagram, e.g., adsorption energy, Gibb's free energy, and potential energy surface, to identify the detail of ORR mechanism and compare the possibility of each intermediates regarding the activation

energies [12, 13]. For example, NØrkskov et al. [14] introduced a simple method to calculate the stability of the reaction intermediates by generating the free-energy profile from the computed binding energy as a function of electrode potential (U), by shifting the free energy of states containing by $-eU$, where e is the electron charge. In their work, a slab model was produced to perform the electronic structure calculation. They suggested that the origin of overpotential was due to O and OH adsorption, while association and dissociation depended on the applied potential and species of metal. Likewise, Sha et al. [15] proposed an application to estimate the optimum operating potential based on the NØrkskov's concept of coupling with external potential (U) taken into account by shifting the free energy of states containing by $-eU$, where e is the electron charge.

Numerous research groups have reported possible reaction pathways of the ORR. One of promising summarization is suggested by Adzic [16] as following;

1. A direct four-electron reduction to the water molecule.

2. A two-electron reduction pathway or the reduction to a hydrogenperoxide.

3. A series pathway with two and four electron reduction.

4. A parallel pathway which consists from step 1. to step 3.

5. An interactive pathway where the diffusion of species from a series path into a direct path is possible.

Furthermore, these reactions rely on the dissociative adsorption process that can be concluded into two elementary steps, which are,

1. A direct four-electron reduction,

$$\begin{aligned} \mathrm{O_2} &\longrightarrow 2\,\mathrm{O_{ad}}, \\ 2\,\mathrm{O_{ad}} + 4\,\mathrm{H^+} + 4\,\mathrm{e^-} &\longrightarrow 2\,\mathrm{H_2O}. \end{aligned} \tag{4.1}$$

2. A peroxide pathway,

$$\begin{aligned} \mathrm{O_2} + 2\,\mathrm{H^+} + 2\,\mathrm{e^-} &\longrightarrow \mathrm{HOOH_{ad}}, \\ \mathrm{HOOH_{ad}} &\longrightarrow 2\,\mathrm{OH_{ad}}, \\ 2\,\mathrm{OH_{ad}} + 2\,\mathrm{H^+} + 2\,\mathrm{e^-} &\longrightarrow 2\,\mathrm{H_2O}. \end{aligned} \tag{4.2}$$

As stated in Chapter 1, there are two molecular models to study the surface geometry theoretically, the slab and the cluster model. Even several works have utilized the slab model to simulate practical condition of metal surface, due to time-consuming in large-size electronic structures computations, effective smaller scale models are thus required for more improvements. Jacob et al. [17] studied the small suitable platinum cluster by BLYP functional and they suggested that the $Pt_{9,10,9}$ structure has the capability for describing all binding site of oxygen molecule on platinum surface. On the other hand, Tao et al. [18] studied the properties of small platinum cluster consisting around 4 to 6 atoms of platinum. They found the capability of DFT methods within such a small-scale system to explain the oxygen adsorption geometry. As well as, in Panchenko's work [19], the DFT calculations using a cluster model of $Pt_9(111)$ were performed and it identified the efficiency of computing the adsorption energy, geometry, and the charge transfer. These studies showed the efficiency of the small system to describe several properties that might be equivalent to larger size computation. Although earlier works efficiently provided the useful results, i.e.,

physisorption and chemisorption structure and intermediates of dissociative adsorption process referring to the binding energy, most of them lacked the electronic properties to evaluate the charge transfer such as ionization potential (IP) and electron affinity (EA), which are significant parameters in terms of requiring energy to withdrawing and adding and electrons to the adsorbate and/or the substrate. Additionally, ORR should be presented in electrical aspect such as I-V characteristics so as to clarify the overpotential problem directly. In this study, the theoretical model [20], which can interpret the charge transfer via a single-molecule junction and treat a non-equilibrium current condition between a molecule and a couple of electrodes, is improved to be applied to the dissociative adsorption of oxygen near the cathode surface of PEMFCs. By focusing on the interaction between molecules and catalytic materials, this model is hoped to applied to analyze the I-V characteristics of PEMFCs associated with the overpotential.

4.2 Methodology

4.2.1 Computational Detail

To begin an initial step of the computational study of ORR on Pt(111) clusters by DFT approach, the effective electronic structure needs to be considered carefully for representing the catalyst surface. Since previous computations indicated that species, shapes, and arrangements of the atoms principally caused the different results. According to our model configuration which principally computes in the atomistic level, the planer cluster model is taken into account since the distribution of metal orbitals might overestimate the computation if the number of molecules in cluster is too much. On the other hand, if the size of cluster is too small, the adsorbate molecule will be coupled with the substrate molecule at the edge because of the dense electrons.

Thereby, the planer cluster should not be too tiny to act as the practical catalyst material. Due to these reasons, the computation system should be represented by the most optimized size of the catalyst cluster.

At first step, to optimize the preferable electronic structures in a catalytic reaction associated with ORR, we perform *ab initio* computations for planer Pt cluster by varying structural parameters such as the number of Pt atoms. First of all, the planer Pt clusters with varying number of atoms are optimized by *ab initio* computations to identify the stable structure of each size of Pt clusters. Secondly, an oxygen molecule is introduced to each optimized Pt clusters to optimize again and the binding energy and adsorption mechanism are defined. Finally, the visualization of calculated system is conducted to illustrate the change in charge density between Pt clusters and oxygen molecule. Next step, to generate the *I-V* characteristics, the neutral system was applied to uniform electric field perpendicular to the Pt cluster plane with the intensity varying from -0.001 to 0.001 V/m. To study the orientation effect, we also adjust the position of the oxygen molecule in direction perpendicular and parallel to the optimized Pt surface at hallow and bridge positions. Finally, the *I-V* characteristics are generated regarding to our theoretical model.

4.2.2 Theoretical Model Improvement

Dissociative adsorption of oxygen molecules onto the platinum surface can be compared to interactions between molecules and an electrode surface [21]. As shown in Figure 4.4, there are two important parameters: the degree of overlap of molecular orbitals (MOs) that describes the state of adsorption and the degree of charging that identifies the strength of coupling regarding to the metal work function, electron affinity, and polarizability. Such parameters are possibly represented by the induced dipole moment. To calculate current due to the charge transfer between a metal cluster and the adsorbed

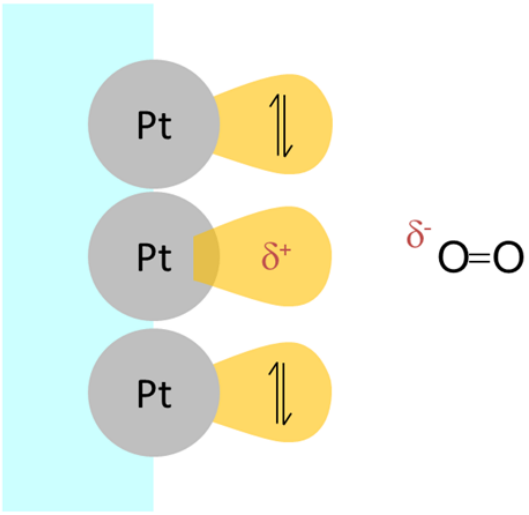

Figure 4.4 Polarization between the adsorbed molecule and the metal surface.

molecule, overlaps of MOs and polarization should be effectively taken into account. Our previous theoretical model [20] that explains the charge transfer in the molecular junction could be improved to apply in this topic. To analyze the I-V characteristics of observed molecule, the computations of current are generated as described in Chapter 2.

However, since the present system consists of a monolayer of cluster, the calculation of voltage difference, ΔV, from Eq. (2.14) has to be revised. In the ORR as stated in Fig. 1.3, oxygen gains the electron from the catalyst, hence the charge transfer comes from Pt cluster to the oxygen molecule. The voltage drop is measured by the difference between the average value of potential of Pt particles and that of oxygen molecule and expressed as follows:

$$\Delta V = \frac{1}{N}\sum_{i=1}^{N}[V_{\mathrm{E}}(\vec{R}_{\mathrm{i}}) - V_0(\vec{R}_{\mathrm{i}})] - \frac{1}{M}\sum_{i=1}^{M}[V_{\mathrm{E}}(\vec{R}_{\mathrm{i}}) - V_0(\vec{R}_{\mathrm{i}})] \tag{4.3}$$

where N and M represent the number of atoms of the Pt cluster and the oxygen molecule, respectively. V is the atomic potential computed by quantum mechanical expectation value as Eq. (2.15).

All calculations are performed using the Gaussian 09 program package [22], by using the Becke three-parameter hybrid functional [23] with the nonlocal correlation of Lee, Yang, and Parr (B3LYP) [24], where douple-ζ basis set with polarization function of Weigend and Ahlrichs, Def2-SVP [25–27] is employed.

4.3 Results and Discussion

4.3.1 Optimization of Pt_n Clusters and Adsorbed Oxygen

Within the theoretical framework [20], the initial configuration of Pt surface is presented by monolayer planer cluster. The Pt_n clusters, where n is the number of Pt atoms, (n= 6, 8, 10 and 12) are studied. Each optimized Pt_n cluster is frozen and located on the xy-plane to optimize again with applied oxygen molecule. The O-O bond lengths in optimization with Pt_6, Pt_8, Pt_{10} and Pt_{12} cluster are 1.39, 1.33, 1.28 and 1.23 Å, respectively. Comparing with the natural single bond length of O-O in gas phase, 1.21 Å [28], the oxygen molecules are elongated in all cases, therefore, the adsorption occurs. However, when the n is below 12 atoms, the oxygen molecule tends to adsorb at the edge of clusters. Although the preferable size of Pt planer surfaces was reported to be up to 9 Pt atoms [29, 30], the results of n = 6, 8 and 10 show that the adsorbate tends to interact with the Pt atoms at the edges. Due to the limitation of DFT method, It may cause too crowded electron density at the borders, so the suitable cluster size should be selected to yield both overcoming the inaccuracy and effectively imitating the actual catalyst surface. The Pt_{12} cluster results in the interaction with the oxygen molecules around the center area as shown in the Fig. 4.5.

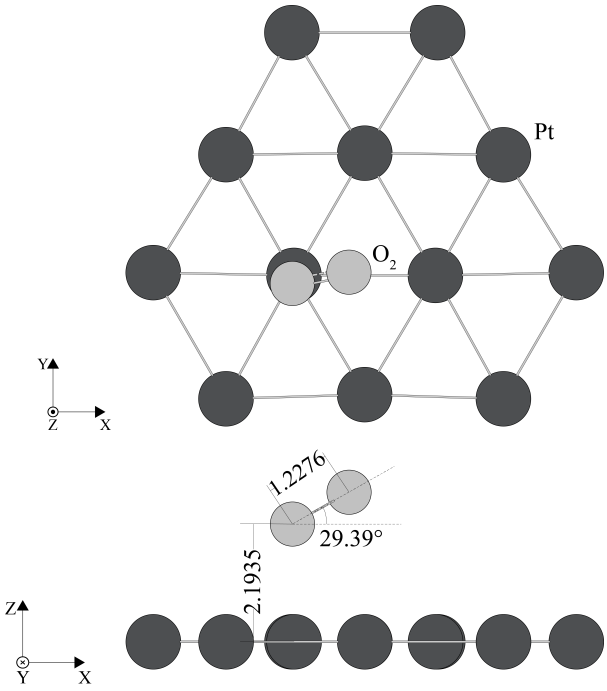

Figure 4.5 Geometry of Pt_{12} cluster with adsorbed oxygen molecule in the xy and xz-planes.

The closer oxygen atom to Pt cluster places at 2.19 Å around the top-site and another is near the bridge site with a little bit apart from the surface. To state the potential to illustrate the practical condition, the adsorption energy is also analyzed as shown in Table 4.1. The result of 0.646 eV is similar to the previous experimental and computational results.

Furthermore, the induced charge density ($\Delta\rho$) is calculated as,

$$\Delta\rho = \rho(Pt_{12}O_2) - \rho(Pt_{12}) - \rho(O_2) \tag{4.4}$$

The distribution of charge density is visualized as Fig. 4.6. It confirms that the the oxygen molecule gains charge when it is dissociatively adsorbed on the Pt cluster. Rising of density of electrons around the oxygen molecule causes the repulsive interaction between each O atom and causes in the bond elongation. Table 4.2 shows the detail of induced charge on each Pt atom and the results imply that the denoted atoms for

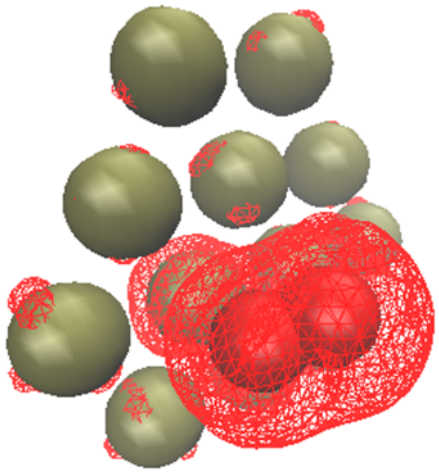

Figure 4.6 Visualization of induced charge density due to the adsorption.

Table 4.1 The adsorption energy of oxygen molecule on Pt surface.

Model and Functional	Adsorption energy (eV)
Experiment [31]	≈0.500
Pt12 cluster model with B3LYP functional	0.646
Four layers slab model with PW91 [19]	0.630
Pt_3 - Pt_6 cluster model with B3PW91	0.53-0.83

charge transfer are mainly the center group. According to all reasons above, hereafter the Pt_{12} cluster is reasonable to perform the computation of charge transfer in the ORR.

4.3.2 Effect of Arrangement of Adsorbed Oxygen

One interesting issue of the adsorption processes on transition metal is the interacting position on catalyst surface. The previous study of ORR on $Pt_9(111)$ concluded that the favorable sites of oxygen adsorption are the hollow and the bridge position [19]. Other previous calculation using a slab model also stated that oxygen molecule tended to be adsorbed on these two sites [32]. Herein, the *I-V* characteristics are analyzed to study the relationship between the adjusted molecular structure and non-equilibrium electrical condition. A distance (d) between the oxygen molecule and Pt surface are

Table 4.2 The induced charge on each atom.

No.	Atom	ρ of adsorption system	ρ of initial system	$\Delta\rho$
1	Pt	-0.538136	-0.377270	-0.160870
2	Pt	0.175299	0.178681	-0.003380
3	Pt	0.046678	0.020311	0.026367
4	Pt	-0.255303	-0.377980	0.122674
5	Pt	0.154889	0.178615	-0.023730
6	Pt	0.204973	0.178890	0.026083
7	Pt	0.135497	0.178737	-0.043240
8	Pt	0.054327	0.019290	0.035037
9	Pt	-0.252461	-0.376620	0.124154
10	Pt	-0.008701	0.019755	-0.028460
11	Pt	0.170670	0.178734	-0.008060
12	Pt	0.152510	0.178849	-0.026340
13	O	-0.012881	0	-0.012880
14	O	-0.027361	0	-0.027360

varied with determining at hollow and bridge positions as shown in Fig. 4.8. Moreover, the oxygen molecule alignment is studied in both perpendicular and parallel directions to the Pt surface. In the optimized structure, the oxygen molecule tends to adsorb onto the cluster at the bridge site horizontally, therefore this structure is set to be a reference one. Figure 4.9 (a) and (b) show the I-V characteristics of bridge and hollow sites on the surface in parallel orientations, respectively. Figure 4.9 (c) and (d) demonstrate those of the system with oxygen in perpendicular direction.

In all cases, results denote that the value of charge transfer when $d = 1$ Å is relatively smaller than the others. This seems to be caused by the localization of frontier MO over the whole system hence the complexity of current computation by energy level of MO. For $d = 2$ Å to 4 Å, the conductance represented by the slope of the graphs becomes lower with d decreasing. It can be explained by the extremely strong coupling between oxygen molecules and Pt atoms where the charge conduction is disturbed and the polarization becomes weak. Meanwhile, the conductance of $d =$

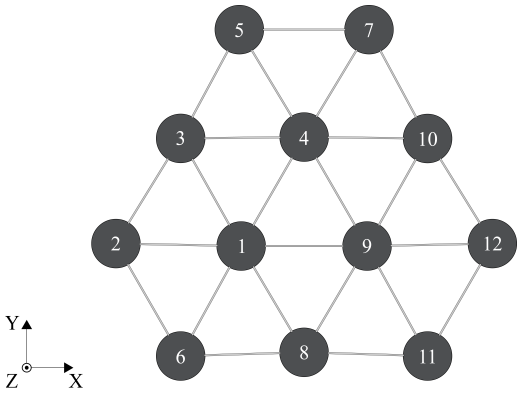

Figure 4.7 Geometry of Pt_{12} cluster with labeling by number according to Table 4.2.

5 Å has highest value. It indicates that in spite of the weak interaction, the change of dipole moment is effective.

To further understand, the HOMO visualizations are illustrated. The one for the case of parallel orientation of oxygen molecule with $d = 1$ Å was evaluated as presented in Fig. 4.10. Regarding to the equilibrium state, it is found that the HOMO broadly extends above both the Pt and oxygen molecule that causes the complex electron bounding and responses weakly to the electric field as shown in Fig. 4.10. On the other hand, the visualizations when $d = 3$ Å in Fig. 4.11 show the clear responding to the direction of electric field. In such a case, the effective conductance tends to be lower, since the electric potential difference becomes large due to the polarization against the electric current. For $d = 5$ Å, Figure 4.12 displays that the MO only localizes on Pt atoms and is not affected by the electric field. Due to apparent separation of MO state between the Pt cluster and oxygen molecule, the potential difference between the two groups becomes lower than the other cases and ΔN and ΔE have small changes resulting in the high conductance. These molecular orbital energy levels are usually affected by the orientation and applied electric field such as the Stark effect and each molecular orbitals localize on various atoms. The orbital coefficients allow us to determine major components on an eigenstate. To discuss quantitatively,

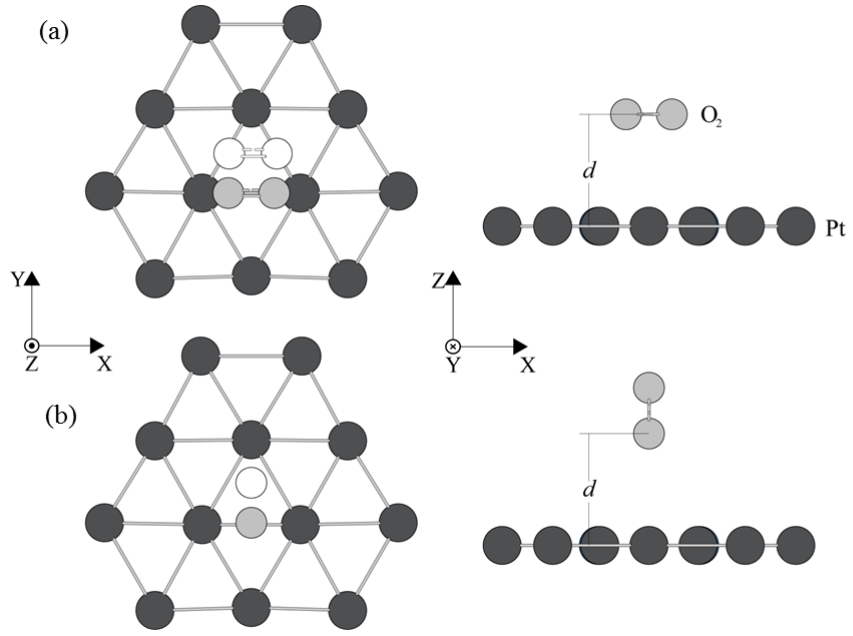

Figure 4.8 Top-view and side-view of Pt_{12} cluster with an adsorbed oxygen molecule at bridge (light gray) and hollow (white) sites fir (a) the parallel orientation and (b) the perpendicular orientation.

Figure 4.13 shows the percentage of the absolute sum of orbital distribution on the oxygen molecules with varying position. The graphs with the high peak of distribution and near the LUMO state define the localization of frontier MO that responds to oxygen molecule. They show that the MO involved electron transfer might be not only HOMO and LUMO but also other frontier levels. This behavior may be one of a significant point in the future development.

In addition, we should further focus the corresponding of molecular orientations to the charge transfer. Figure 4.14 presents the I-V characteristics of the hollow and bridge sites in horizontal and vertical adsorption. The difference in the orientation is identified evidently, even though the results from different adsorption sites cannot be clearly distinguished. The conductance of composition with the oxygen molecule in perpendicular orientation is higher than that of the parallel orientation. This

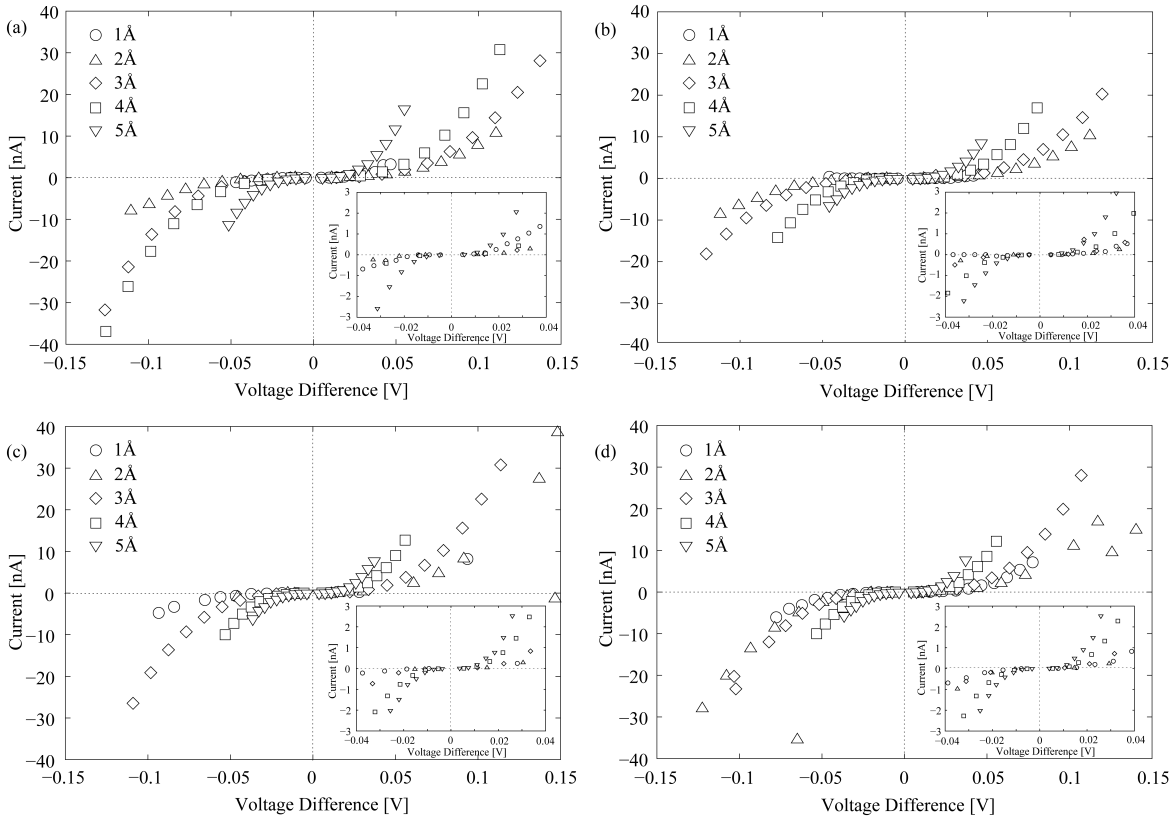

Figure 4.9 *I-V* characteristics for parallel orientation of oxygen adsorbed at (a) bridge site and (b) hollow site as shown in Fig. 4.8; that for perpendicular orientation adsorbed at (c) bridge site and (d) hollow site. Magnified views ranging from -0.1 to 0.1 V are shown in insets.

demonstration is in agreement with the movement direction of electron in the electronic structure, when adsorbed particle is vertically aligned to the catalyst plane. As a result, the charge from Pt can be more easily transported to oxygen. In addition, from the energetical point of view, the parallel orientation at the bridge site is the most stable thus the interaction is strong between the two materials. The overlaps of MOs cause a strong polarization and generate a large potential difference in uniform electric fields resulting in the lower conductance.

In conclusion, the results of optimized system of Pt_n cluster and the oxygen molecule show that the suitable structure to model the charge transfer is Pt_{12} cluster. The charge density is induced by the adsorption process and the oxygen gains the charge from the

Pt cluster which can indicate the trends of physical and chemical adsorption. Moreover, the distance between the oxygen atoms is elongated according to the chemisorption. The I-V characteristics are conducted for systems varying the position and arrangement of adsorbed oxygen molecule. The results can demonstrate the different orientation and reasonably explain the conductance change.

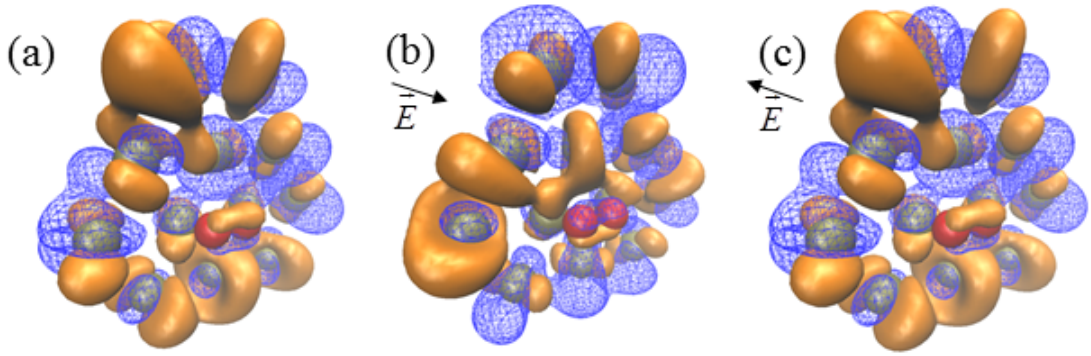

Figure 4.10 Visualization of HOMO when oxygen is located at 1 Åfrom the Pt surface at the bridge site in parallel orientation, (a) without electric field, (b) with positive electric field, and (c) with negative electric field along the z-axis. MOs are presented at isovalue of 0.01 (solid for positive and meshed for negative values).

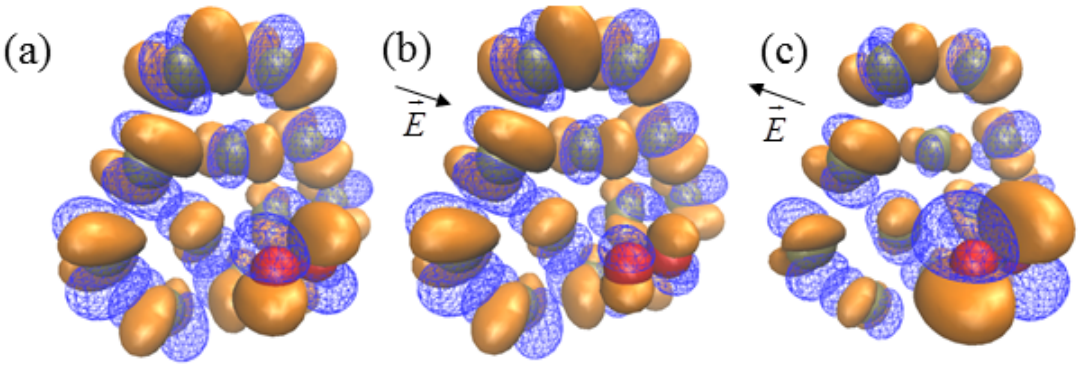

Figure 4.11 Visualization of HOMO when oxygen is located at 3 Åfrom the Pt surface at the bridge site in parallel orientation, (a) without electric field, (b) with positive electric field, and (c) with negative electric field along the z-axis. MOs are presented at isovalue of 0.01 (solid for positive and meshed for negative values).

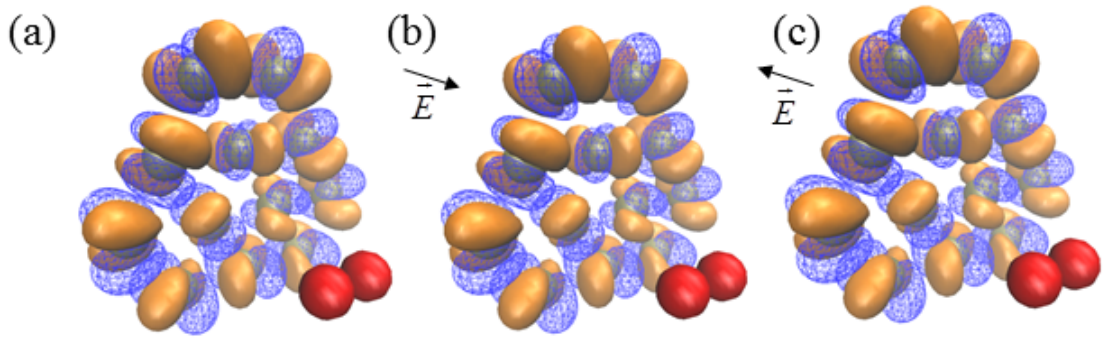

Figure 4.12 Visualization of HOMO when oxygen is located at 5 Åfrom the Pt surface at the bridge site in parallel orientation, (a) without electric field, (b) with positive electric field, and (c) with negative electric field along the z-axis. MOs are presented at isovalue of 0.01 (solid for positive and meshed for negative values).

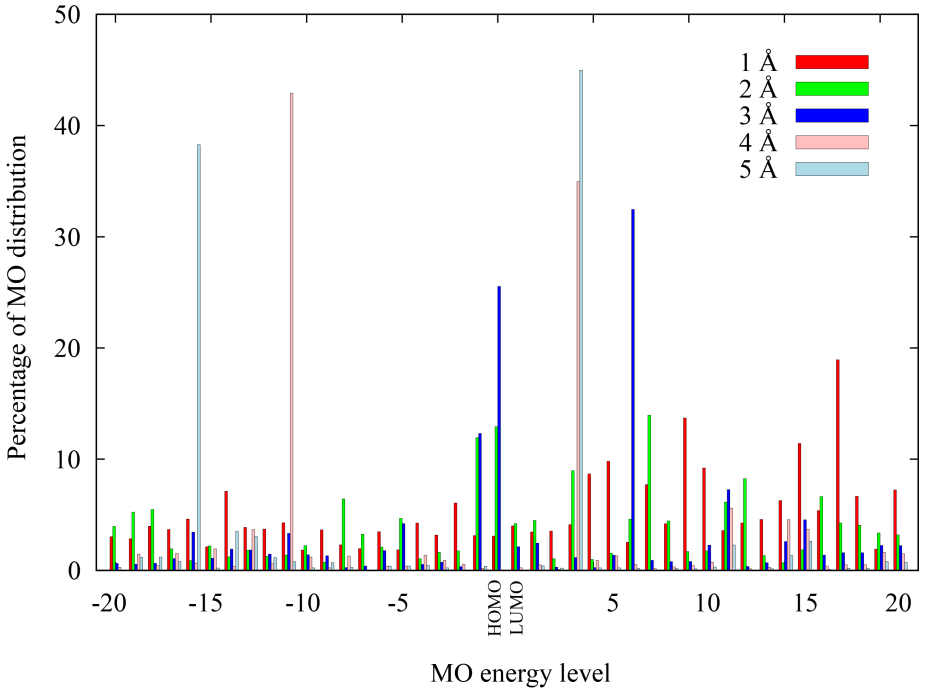

Figure 4.13 The percentage of molecular orbital distribution on oxygen molecule located at varied distance from Pt cluster.

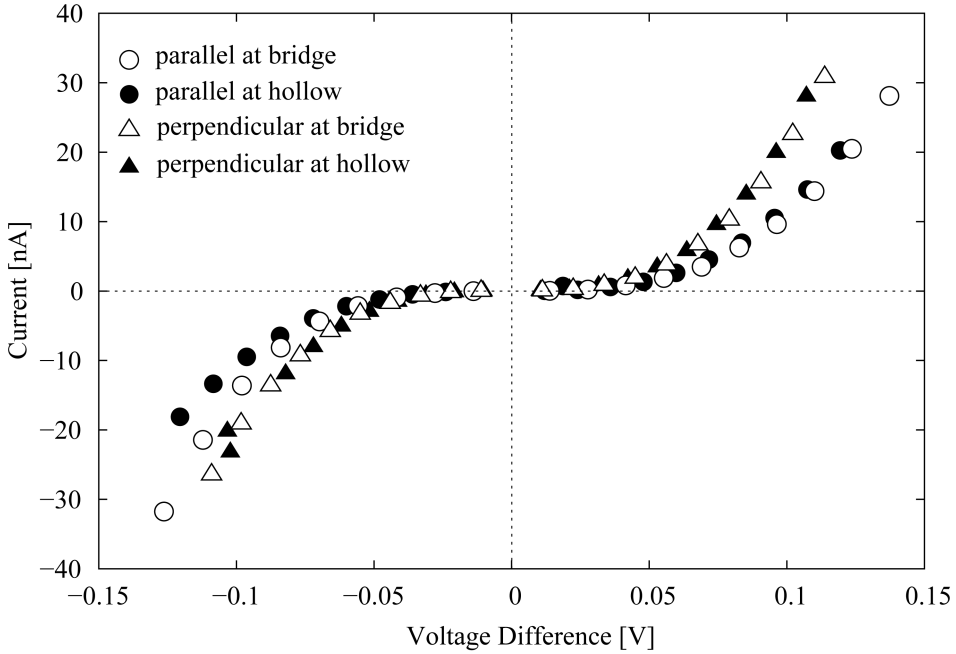

Figure 4.14 I-V characteristics for $d = 3$ Å at various orientations.

4.4 Perspective in Future Works

To study the larger size of computation such as solvent model or generate the continuous movement similar as the practical electrochemical reactions, *ab initio* approaches are limited to apply since they are performed overall interactions including nuclear-nuclear, nuclear-electron and electron-electron. Therefore, molecular dynamics simulations that based on conventional mechanics are emphasized in the electrochemical computation, especially the complex reaction on metal electrodes [33, 34]. Combining the quantum and molecular mechanics, the *ab initio* molecular dynamics (AIMD), or called as quantum mechanics/molecular mechanics (QM/MM) methods, is introduced, for example, in the Car-Parrinello methods [35]. The AIMD utilizes the acting force within quantum calculations which provides atomistic results then uses this interacting information to gain the position of atoms computed by the classical Newton's equations of motion as simply summarized in Fig. 4.15.

To further improve our study [36] for realistic ORR pathways, the AIMD approach has been carried out in this topic. Earlier works [37, 38] basically represented the detailed mechanism of the ORR in terms of MD trajectories and their propose was to point out the charge transfer step in the ORR via energy profile. Furthermore, the simple electron and ion dynamics during the dissociative adsorption of oxygen on metal surface were studied by Y. Suzuki et al. [39]. Their work carried out the Ehrenfest time-dependent density functional theory (TDDFT) molecular dynamics simulation to compare the catalytic activities of Pt and Au clusters. The result identified the occurrence of electron transfer and showed the initial step to improve the AIMD simulation. In addition, the structural adsorption is able to simulate by classical MD. The recent work by Li et al. [40] studied the stable of oxygen and water molecules adsorbed on Pt layer using slab model with classical MD approach. Their result suggested the stable arrangement in a parallel direction to the cluster

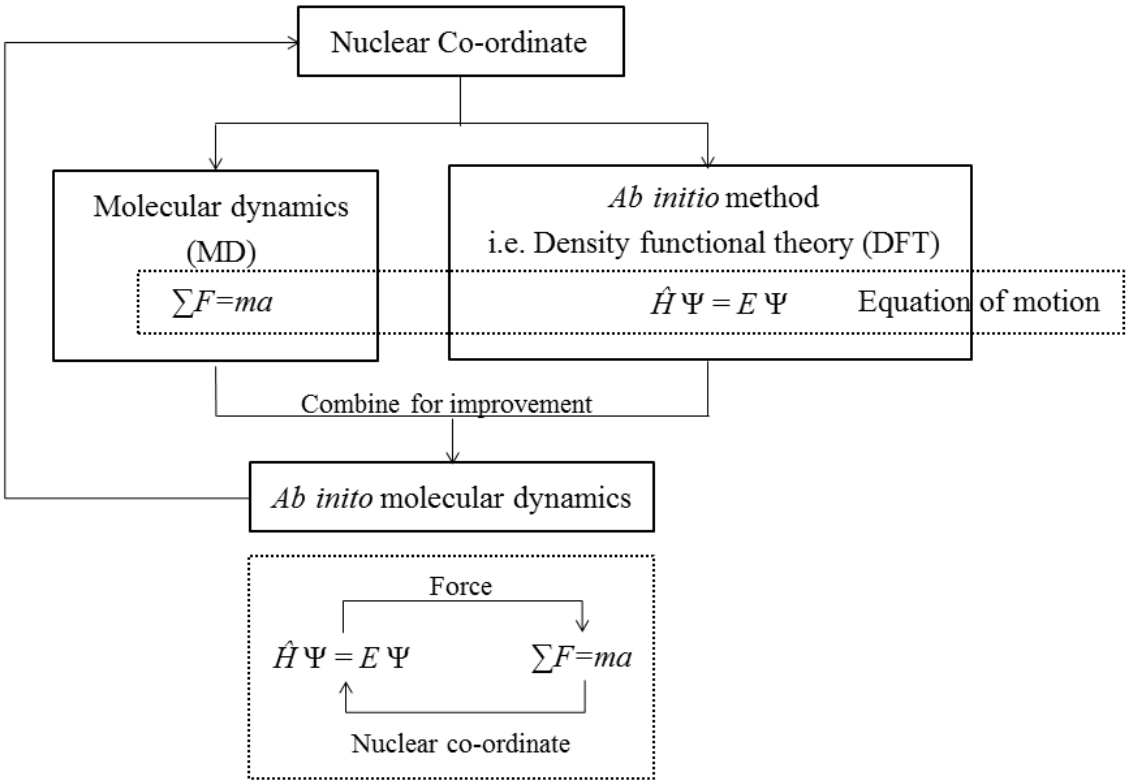

Figure 4.15 Concept of *ab initio* molecular dynamics.

surface as our previous optimization by DFT approach [36]. In addition, the AIMD method has been applied to the alternative catalyst material topics. Okamoto [41] performed the AIMD to simulate various ORR pathways on the alternative catalyst which provided the continuous information to plot potential energy surface (PES) on non-metal material i.e. ZrO_2 and nitrogen-doped carbon. The qualitative results were suggested satisfactorily, however, he stated the main two difficulties to employ the MD for the reduction reaction. One is the method to apply the potential to the system and the other problem is the limitation of computer resources.

As DFT result in Fig. 4.9, the conductance of systems with varying distance between adsorbed oxygen and Pt cluster shows complicated trend. Hence, the continuous

movement of dissociative adsorptions could elucidate this incorrectness. One of the electron properties that might be changed during the reaction is the spin of adsorbed oxygen. The spin transition is reported in the study with the metal surface [42] and nitrogen-doped carbon nanotube [43]. In order to describe previous ambiguous results, we analyze the effect of spin change during the adsorption process as well as further perform the AIMD to evaluate the electrical profiles for the continuous intermediates of ORR.

4.4.1 Study of spin state transition

Our earlier consideration covered only the singlet oxygen molecule, whereas, the most stable state of the isolated oxygen molecule is the triplet state. For example, the oxygen molecule located far from platinum cluster should be assumed in the triplet state and one interacted with the metal surface might be changed to singlet state. The complexity of molecular orbital of triplet oxygen are illustrated in Fig. 4.16. In $2\pi_p^*$ molecular orbital, there are six possibilities to arrange the two residual valence electrons, thus, it is called triplet state.

The effect of the spin state transition of oxygen molecule is analyzed while the molecule is dissociatively adsorbed on the planer platinum cluster. Since the functional of DFT method and basis set, which have variety of parameters to describe various electronic structures and their electron state, need to be validated to confirm the possibility for the triplet state calculation. Hence, we compute the single point calculations of the previous condition and the other which are suitable to study the electron transfer, i.e., TPSS functional method and LANL2DZ-ECP basis set. Then, to simulate the adsorption pathway, the potential energy curves (PEC) are generated for both singlet and triplet states to specify the variation of spin of oxygen molecule relating to the electronic energy and the distance between the oxygen molecule and platinum

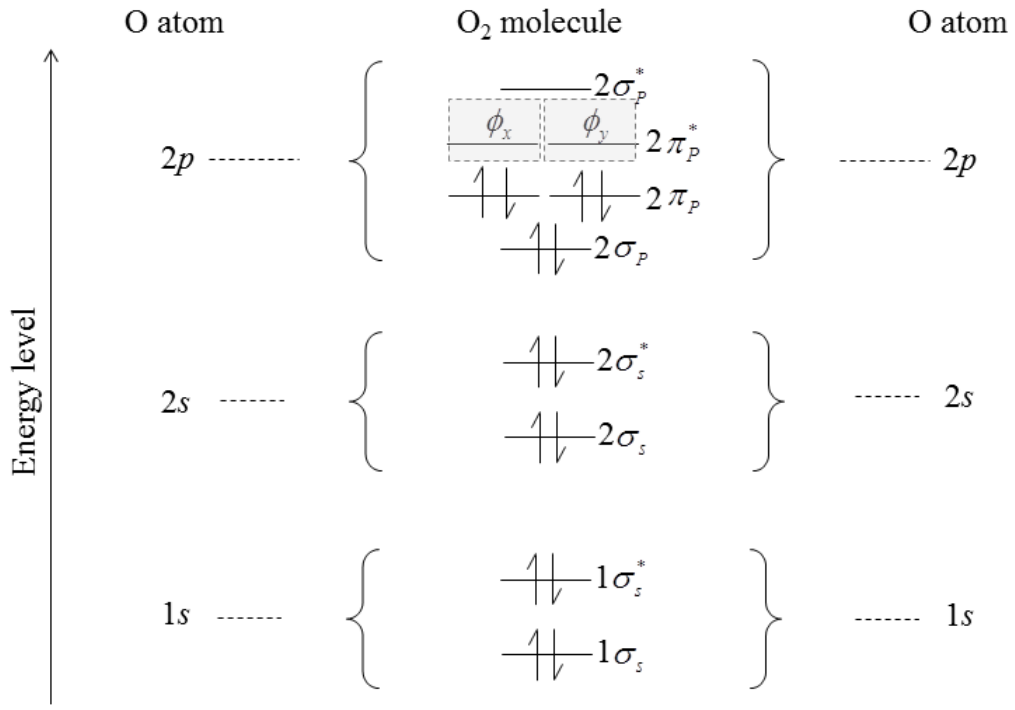

Figure 4.16 Molecular orbital energy level of the triplet oxygen [12].

cluster. However, there are difficulties in calculations of triplet state system, thus, the computational conditions have to be adjusted manually, i.e., convergence criteria and the molecule co-ordinate, etc., for each computation. This will be burdensome in the case of AIMD simulation, therefore, the DFT calculation has to be simplified such as the quadratically convergent SCF procedure [44].

To decrease computational time-consuming, the three atoms of platinum cluster with one oxygen molecule for computational system are used. All the DFT calculations are performed by using Gaussian 09 program pack [22]. The density functional in comparison are hybrid B3LYP, which combines the Becke three-parameter hybrid functional [23] with the nonlocal correlation of Lee, Yang, and Parr [24], and TPSS exchange-correlation functional of Tao, Perdew, Staroverov, and Scuseria's work [45]. For the basis set, we apply the Def2-SVP basis set using douple-ζ set with polariza-

tion function of Weigend and Ahlrichs [46, 47] and LANL2DZ using effective core pseudopotentials of double-ξ type [48–51].

Since the spin transition from triplet to singlet state occurs via complex alignment in molecular orbitals, the computational method and basis set are required to confirm their capability delicately. The B3LYP functional with the Def2-SVP basis set was used in our previous calculations, furthermore, the TPSS functional with the LANL2DZ basis set is recommend to use in study relating to the electron transfer. Therefore, these conditions are compared. We should recall to the virial theorem which stated the relation of the average kinetic energy and average potential energy of the total system. This theory shows that at the ground state the total energy is equal to one-half of the average potential energy and the average kinetic energy is equal to the total energy with the sign changed [52]. It can be briefly derived as;

$$2T = V \tag{4.5}$$

where T is the kinetic energy and V represents the potential energy. The $(-\frac{V}{T})$ is called virial ratio and theoretical value is 2. Moreover, to validate the spin state, we must validate the measurable quantity of the spin which is the square of spin length (S^2). Since spin is the internal angular momentum of particle, only particular value can be observed. The S^2 is state by eq. (4.6) [53].

$$S^2 = s(s+1)\hbar^2 \tag{4.6}$$

where s is the spin quantum number and $\hbar$ is the reduced Planck constant. For the singlet state, the s is equal to zero, thus its S^2 become zero also. For the triplet, the s is equal to one, hence the S^2 is 2.

Table 4.3 Comparison of computational conditions.

Functional method	Basis set	$(-\frac{V}{T})$	S^2
B3LYP	Def2-SVP	3.4855	3.3465
	LANL2DZ	3.4854	3.3181
TPSS	Def2-SVP	3.4921	4.0280
	LANL2DZ	2.9293	3.0296
Theoretical Value		≈ 2.0000	2.0000

As in the Table 4.3, the computational results are compared with those of the theoretical value. The quantities of B3LYP functional are overestimated in all cases of basis set, that confirms the inaccurate conductance in our previous works. Anyway, the TPSS functional with LANL2DZ basis set provides most favorable value of the virial ratio and the S^2, thus this identifis the efficiency to use in the triplet oxygen computation. Furthermore, we generate the visualization of the spin density of whole system and that of the isolated triplet oxygen to illustrate the spin state as in Figure 4.17. Both shapes of spin are coincided with each other, so that this method gives reasonable computation of the triplet oxygen adsorbed onto the platinum cluster.

The potential energy surface has been widely used to explain the interaction of oxygen on metal surface since it can identify the structure energy variation at each step of electrochemical reaction. The potential energy surface is computed by TPSS functional with LANL2DZ level of theory. The computed structure consists of the three atoms of platinum cluster and one oxygen molecule arranged in parallel orientation to the platinum cluster. The center of mass of oxygen molecule is aligned with that of platinum group and the distance, d, between oxygen molecule and platinum cluster are varied as shown in Fig. 4.18. Since the triplet oxygen is known as the stable state of isolated molecule, as well as, its singlet is represented within the excited state, we decide the different way to produce the potential energy curves for each spin state. In triplet case, we start at $d = 5$ Å, and then decrease the distance to come closer to platinum cluster, hence the adsorption. On the other hand, we begin at the closest position

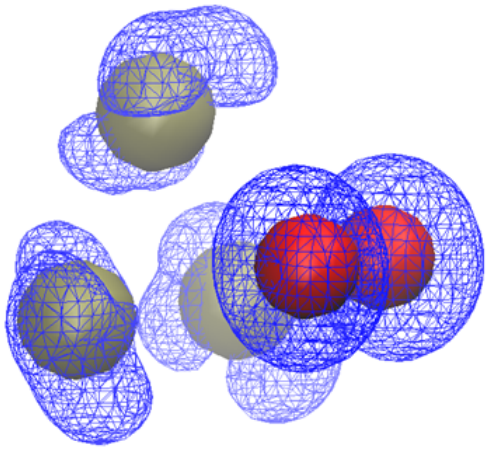

(a) Spin density of system

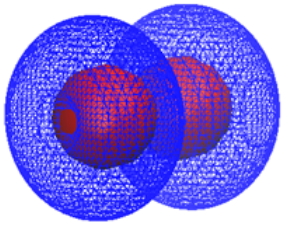

(b) Spin density of triplet oxygen

Figure 4.17 Visualization of spin density.

to the platinum layer (d=1 Å) for singlet oxygen, so as to imitate the desorption of excited molecule.

As presented in Figure 4.19, the energy of singlet system is little higher than that of triplet when d over 2 Å, hence, the adsorption of the singlet is more difficult. However, the computation considering triplet oxygen has some crucial problems. That is, the self-consistent field loop of DFT is arduous to get the convergence because the convergence criterion is not met. Hence, the convergence criteria value and other conditions, e.g., molecule co-ordinate for each calculation have to defined manually. We might neglect the effect of spin in conclusion.

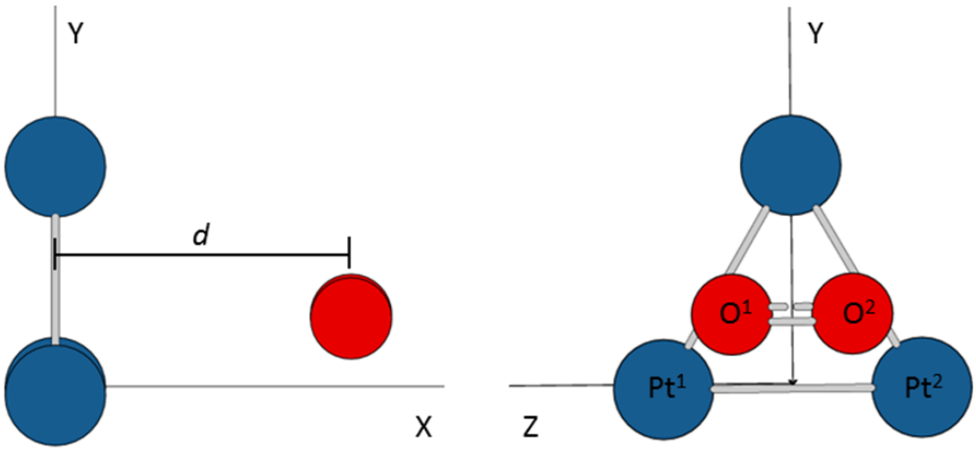

Figure 4.18 A configuration of computational system with adsorbed oxygen.

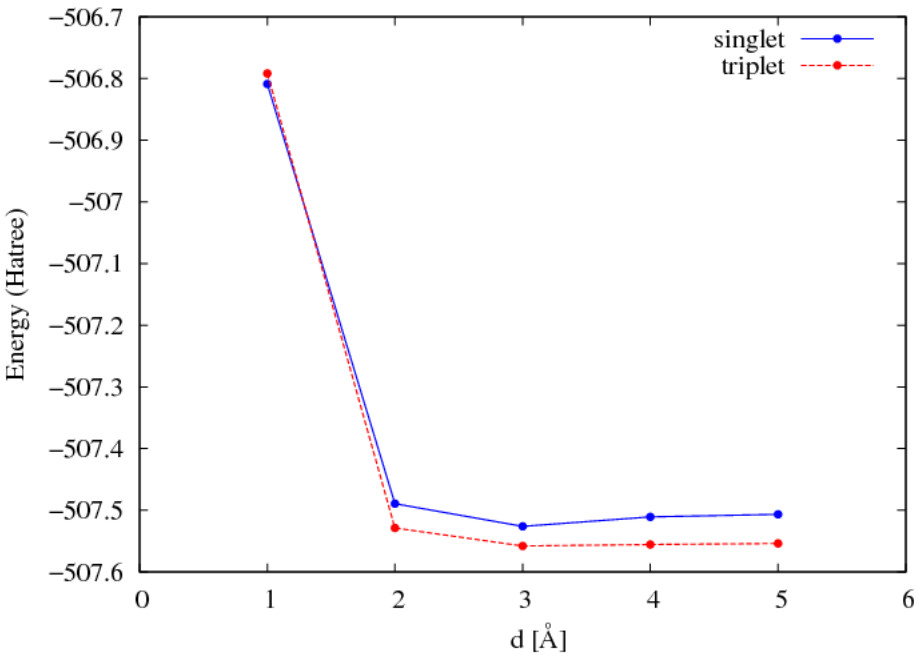

Figure 4.19 The potential energy curve of the triplet and singlet oxygen adsorbed on the platinum surface.

4.4.2 *Ab initio* Molecular Dynamics to Study on Intermediates of ORR

Owing to our group's previous work that can effectively investigate the dissociative adsorption of hydrogen on the surface of graphene [54], this simulation is performed to get the intermediate steps of ORR and the developed theoretical model [20, 36] is taken into account to evaluate the I-V characteristics for particular computed structures which are significant in reaction process.

About the molecular dynamic simulation, the trajectories of particles are calculated by the Verlet algorithm. It integrates of Newton's equation of motion by Taylor's expansion as following [55];

$$\begin{aligned} r_{x,i}(t+\Delta t) &= r_{x,i}(t) + v_{x,i}(t)\Delta t + \frac{1}{2}a_{x,i}(t)\Delta t^2, \\ r_{y,i}(t+\Delta t) &= r_{y,i}(t) + v_{y,i}(t)\Delta t + \frac{1}{2}a_{y,i}(t)\Delta t^2, \\ r_{z,i}(t+\Delta t) &= r_{z,i}(t) + v_{z,i}(t)\Delta t + \frac{1}{2}a_{z,i}(t)\Delta t^2, \end{aligned} \tag{4.7}$$

when $r_{x,i}$, $r_{y,i}$ and $r_{z,i}$ are the function of position of the particle i^{th} at time t in direction x, y and z, respectively. $v_{x,i}$, $v_{y,i}$ and $v_{z,i}$ are the velocity of the molecule i^{th} which can be derived as,

$$\begin{aligned} v_{x,i}(t+\Delta t) &= v_{x,i}(t) + \frac{1}{2}(a_{x,i}(t+\Delta t) + a_{x,i}(t))\Delta t, \\ v_{y,i}(t+\Delta t) &= v_{y,i}(t) + \frac{1}{2}(a_{y,i}(t+\Delta t) + a_{y,i}(t))\Delta t, \\ v_{z,i}(t+\Delta t) &= v_{z,i}(t) + \frac{1}{2}(a_{z,i}(t+\Delta t) + a_{z,i}(t))\Delta t, \end{aligned} \tag{4.8}$$

when $a_{x,i}$, $a_{y,i}$ and $a_{z,i}$ are the acceleration of the i^{th} particle at time t in each direction. These accelerations are computed by the force generated by DFT approach.

Two of the most interesting reactants of the first intermediate of ORR used in previous computational studies are the O_2 and OOH adsorbed on the Pt surface [56]. However, to simplify the primary step, the computation system consists of 12 Pt atoms planer cluster with adsorbed OOH and the approaching H ($(OOH)_{ad}$+H/Pt_{12}), when $_{ad}$ denotes for the adsorbed particle, is studied as the beginning structure of the *ab initio* MD simulation. To ensure the dissociative adsorption, the isolated H atom is introduced with initial kinetic energy that at least equals to the binding energy of adsorbed particles on Pt surface [57] to express the dissociation. As representative of catalyst surface, the Pt_{12} cluster, which optimized with adsorbates within the DFT framework, is frozen during the dynamic calculation.

Our MD simulation is considered in constant temperature condition due to relatively small computational time in 10^{-15} second scale, hence, the effect of temperature can be neglected. The DFT method is employed with the hybrid B3LYP functional, which combines the Becke three-parameter hybrid functional [23] with the nonlocal correlation of Lee, Yang, and Parr [24]. The LANL2DZ basis set with effective core pseudopotentials of double-ζ type [48–51] is used. All the DFT calculations are performed by using Gaussian 09 program pack [22], coupling with an in-house developed MD procedure. Using the velocity Velret algorithm, a time step $\triangle t$ is set to 0.5 fs as refer to our previous study [54]. For the *ab initio* MD results, *I-V* characteristics are evaluated across transition states that involve in the charge transfer.

The first computation step starts with electronic structure as shown in Fig. 4.20 (a) and (b). Initially, H2 is located 3 Å away from the O2 where its molecular axis is perpendicular to the Pt cluster and center of mass of H2 coincides with that of O2. Since the closest atom to H2 is O1 at the initial condition and O1 has more negative charge owing to the OH bond, H2 is strongly attracted to O1-H1 to form the water molecule. As shown in Figure. 4.22, the obvious dissociation of O1-O2 occurs at 60

fs which the bond length become over 2 Å. Although H2 and O1 are closer with the distance below 1 Å at time around 30 fs, there are the fluctuation due to coloumb force during all time step therefore H_2O rotates after its formation as displayed in Fig. 4.21.

To study the electron transfer, the *I-V* characteristics are generated under applied electric field as Fig. 4.23. The results at t below 50 fs show complicated trend that caused by the close position of the donor and the acceptor of electron transfer. The initial structure (t=0 fs) under the applied negative electric field has the relatively high current. This overestimation can be explained by the O2-H2 at original position which aligns parallel to the electric field direction, hence the immense polarization to the Pt cluster. In the early computational time step, both adsorbed groups and cluster still have strong polarization to each other, thus, the electron transfer is major dominated by the high electronegativity of molecules instead of the dependence of external electric field. Basically, Pt atoms donate electrons to the adsorbate molecules and such electron transportation evaluate the symmetrical *I-V* characteristics [36]. The symmetry graph occurs when t equals to 60 fs that near the intercept point of O1-O2 and Pt-O2 in Fig. 4.22. Since the slope of *I-V* curve represents the conductance, one with higher slope indicates that electron can pass though easier. The conductance is highest when $t = 75$ fs since the O1-H1 nearly align vertically to the Pt surface, where angle of H1-O1-H2 = 107.51°, that caused larger possibility of electron transfer. Furthermore this conductance is higher than that of $t = 60$ fs, it identifies the lower possibility of electron movement when the atoms form to the isolated molecules.

In conclusion, our previous AIMD simulation is improved in order to simulate the basic intermediates of ORR. Furthermore, the important reaction steps which identify about ORR mechanism are analyzed by *I-V* characteristics generated by our developed

theoretical model [36]. The present electric profiles can identify the trend of electron transfer.

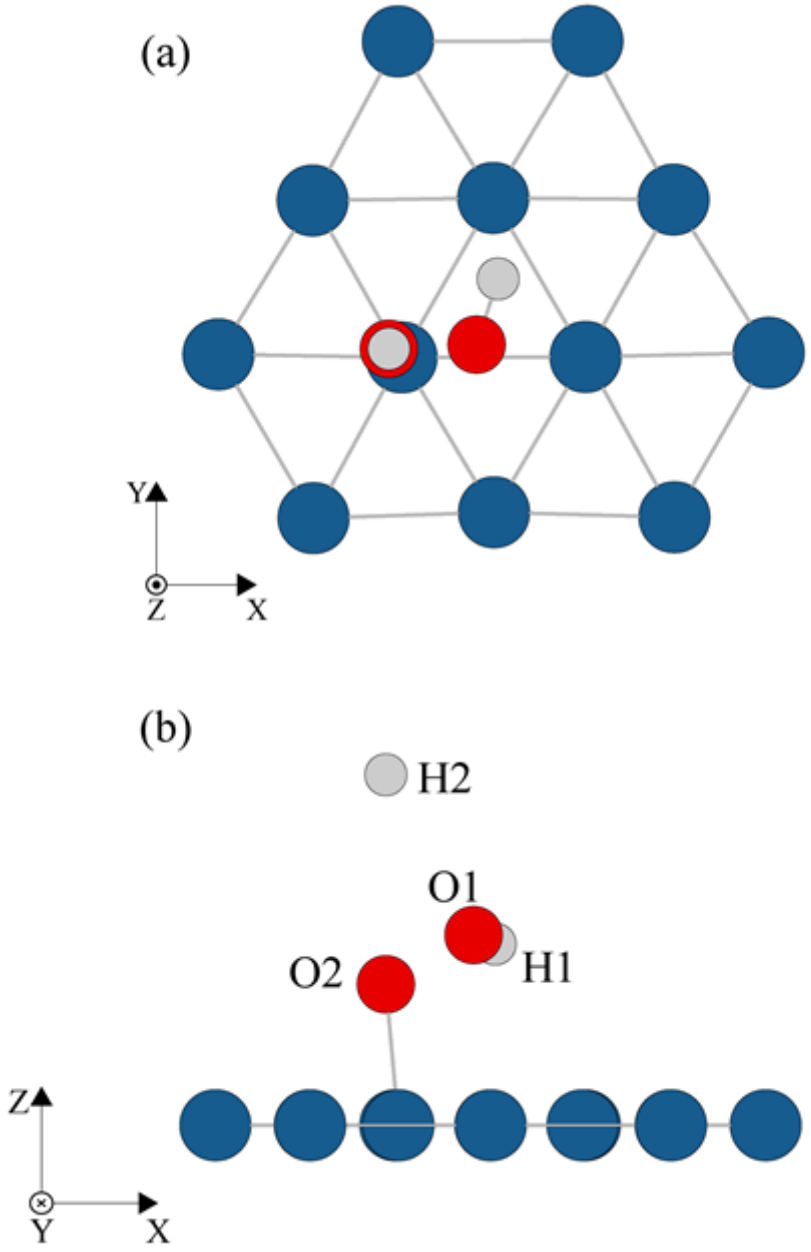

Figure 4.20 Initial geometry of structure consisted of OOH and Pt_{12} in (a) the *xy*-plane and (b) the *xz*-plane.

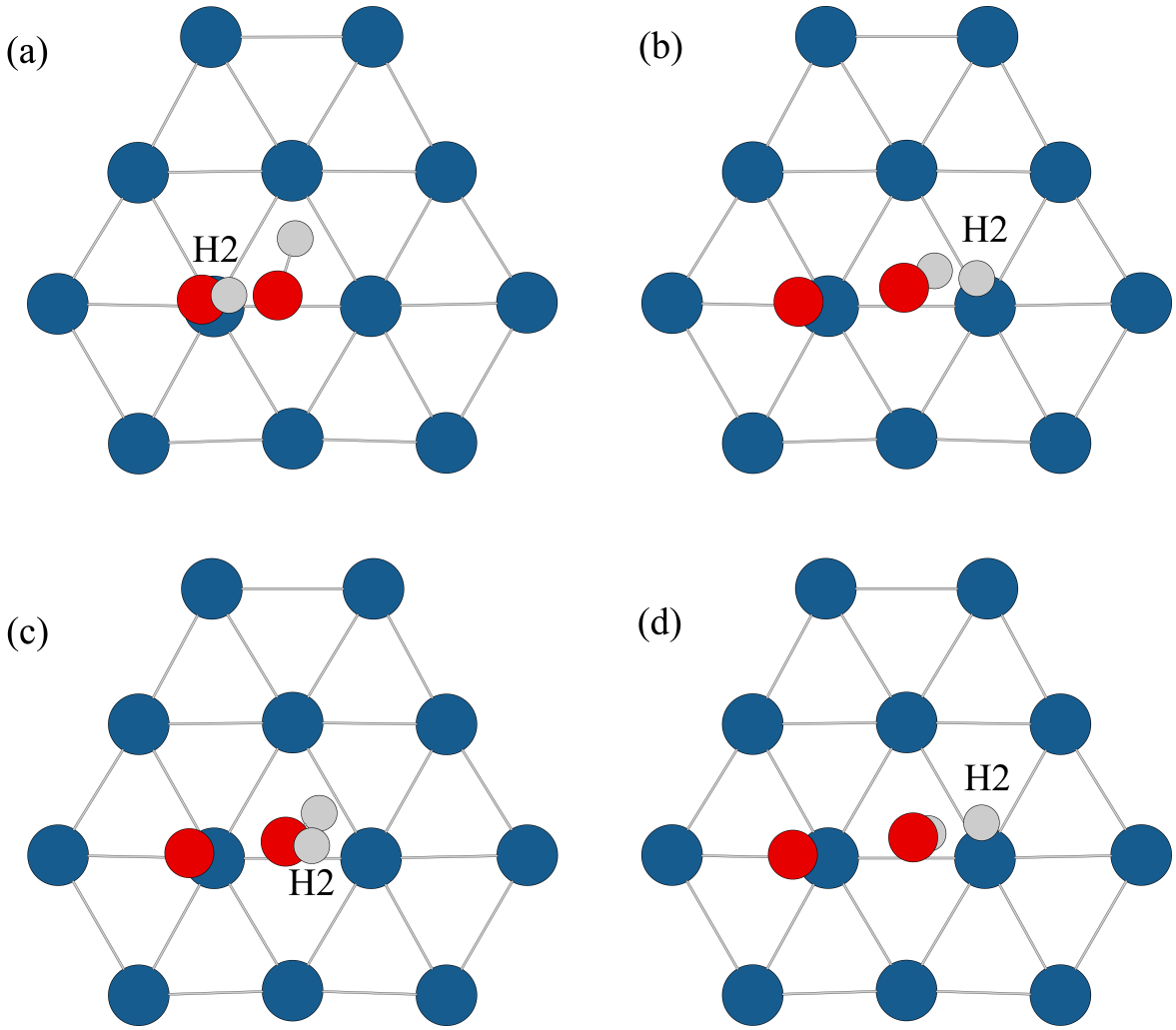

Figure 4.21 Snapshots of the computational system at (a) $t = 25$ fs, (b) $t = 50$ fs, (c) $t = 60$ fs, and (d) $t = 75$ fs.

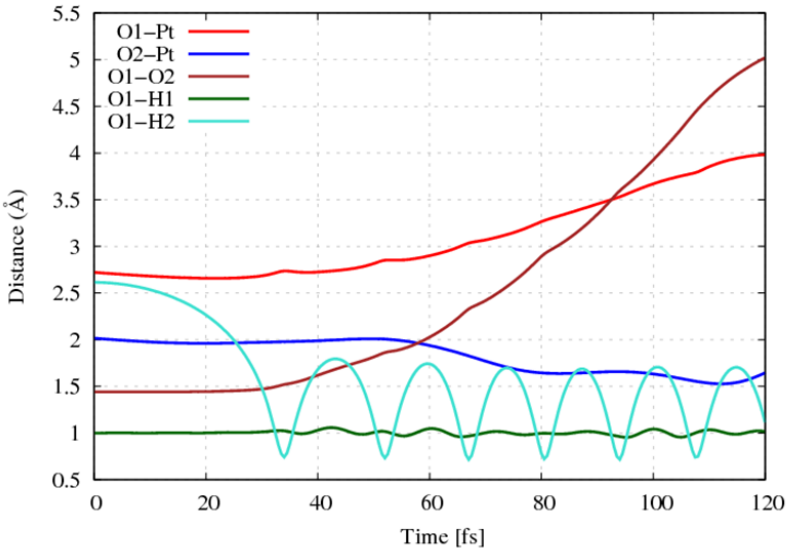

Figure 4.22 Time evolutions of distance between atoms.

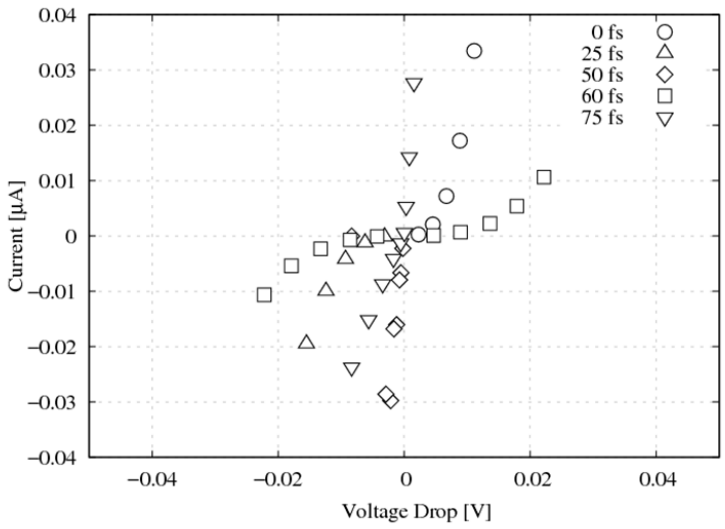

Figure 4.23 I-V characteristics of particular reaction states.

References

[1] J. Larminie and A. Dicks. *Fuel Cell Systems Explained*. 2nd ed. Wiley–VCH, Inc., 2003.

[2] C. Song and J. Zhang. "Electrocatalytic Oxygen Reduction Reaction". In: *PEM Fuel Cell Electrocatalysts and Catalyst Layers*. Ed. by Jiujun Zhang. Springer London, 2008. Chap. 2, pp. 89–134.

[3] S. Gottesfeld. "Electrocatalysis of Oxygen Reduction in Polymer Electrolyte Fuel Cells: A Brief History and a Critical Examination of Present Theory and Diagnostics". In: *Fuel Cell Catalysis: A Surface Science Approach*. Ed. by T. M. Koper. Hoboken, NJ, USA: ohn Wiley Sons, Inc., 2009. Chap. 1, pp. 1–39.

[4] A.Z. Weber and J. Newman. "Modeling Transport in Polymer-electrolyte Fuel Cells". In: *Chemical Reviews* 104.10 (2004), pp. 4679–4726.

[5] N. Cherdsanguan et al. "Analysis of Platinum Particle–size Effect on Performance of PEFCs Using Modeling Approach". In: *Proceedings of the 2nd TSME International Conference on Mechanical Engineering (TSME-ICOME)*. 2012, pp. 1–7.

[6] N. Limjeerajarus and T. Yamaguchi. "Effect of Platinum Particle Size on Catalyst Activity in Practical Gas-phase PEFC MEAs". In: *Proceedings of the 8th International Conference on Fuel Cell Science, Engineering, and Technology*. 2010.

[7] T. Toda et al. “Enhancement of the Electroreduction of Oxygen on Pt Alloys with Fe, Ni, and Co”. In: *Journal of the Electrochemical Society* 146.10 (1999), pp. 3750–3756.

[8] K. Gong et al. “Nitrogen-doped Carbon Nanotube Arrays with High Electrocatalytic Activity for Oxygen Reduction”. In: *Science* 323.5915 (2009), pp. 760–764.

[9] A.C. Luntz, M.D. William, and D.S. Bethune. “The Sticking of O_2 on a Pt(111) Surface”. In: *Journal of Chemical Physics* 89.7 (1988), pp. 4381–4395.

[10] T. Zambelli et al. “Complex Pathways in Dissociative Adsorption of Oxygen on Platinum”. In: *Letters to Nature* 390 (1997), pp. 495–497.

[11] J.R.D. Lile and S. Zhou. “Theoretical Modeling of the PEMFC Catalyst Layer: A Review of Atomistic Methods”. In: *Electrocimica Acta* 177.24188 (2015), pp. 4–20.

[12] A. Groß. *Theoretical Surface Science: A Microscopic Perspective*. Springer Berlin Heidelberg., 2009.

[13] Z. Shi et al. “Current Status of Ab Initio Quantum Chemistry Study for Oxygen Electroreduction on Fuel Cell Catalysts”. In: *Electrocimica Acta* 51 (2006), pp. 1905–1916.

[14] J. K. Nørskov et al. “Origin of the Overpotential for Oxygen Reduction at a Fuel-Cell Cathode”. In: *Journal of Physical Chemistry B* 108.46 (2004), pp. 17886–17892.

[15] Y. Sha et al. “Prediction of the Dependence of the Fuel Cell Oxygen Reduction Reactions on Operating Voltage from DFT Calculations”. In: *Journal of Physical Chemistry C* 116.10 (2012), pp. 6166–6173.

[16] Adzic RR. “Electrocatalysis”. In: ed. by J. Lipkowski and P.N. Ross. Wiley–VCH, Inc., 1998. Chap. 5, p. 197.

[17] T. Jacob, R.P. Muller, and W.A. Goddard III. "Chemisorption of Atomic Oxygen on Pt(111) from DFT Studies of Pt-Clusters". In: *Journal of Physical Chemistry B* 107.35 (2003), pp. 9465–9476.

[18] T. Li and P.B. Balbuena. "Computational Studies of the Interactions of Oxygen with Platinum Clusters". In: *Journal of Physical Chemistry B* 105.41 (2001), pp. 9943–9952.

[19] A. Panchenko et al. "Ab Initio Calculations of Intermediates of Oxygen Reduction on Low-Index Platinum Surfaces". In: *Journal of The Electrochemical Society* 151.12 (2004), A2016–A2027.

[20] P. Szarek et al. "Theoretical Study on Physicochemical Aspects of a Single Molecular Junction: Application to the Bases of ssDNA". In: *Journal of Physical Chemistry B* 117 (2013), pp. 10809–10817.

[21] Nivaldo J. Tro. *Chemistry : A Molecular Approach*. 2nd ed. Pearson, 2011.

[22] M. J. Frisch et al. *Gaussian09 Revision D.01*. Gaussian Inc. Wallingford CT 2009.

[23] A. D. Becke. "Density-Functional Thermochemistry. III. The Role of Exact Exchange". In: *Journal of Chemical Physics* 98 (1993), pp. 5648–5652.

[24] C. Lee, W. Yang, and R. G. Parr. "Development of the ColleSalvetti Conelation Energy Formula into a Functional of the Electron Density". In: *Physical Review B* 37 (1988), pp. 785–789.

[25] F. Weigend and R. Ahlrichs. "Balanced Basis Sets of Split Valence, Triple Zeta Valence and Quadruple Zeta Valence Quality for H to Rn: Design and Assessment of Accuracy". In: *Physical Chemistry Chemical Physics* 7 (2005), pp. 3297–3305.

[26] D. Feller. "The Role of Databases in Support of Computational Chemistry Calculations". In: *Journal of Computational Chemistry* 17 (1996), pp. 1571–1586.

[27] K. L. Schuchardt et al. “Basis Set Exchange: A Community Database for Computational Sciences”. In: *Journal of Chemical Information and Modeling* 47 (2007), pp. 1045–1052.

[28] W. M. Haynes. *CRC Handbook of Chemistry and Physics*. 91st ed. CRC Press (Taylor and Francis Group), 2010.

[29] L. Xiao and L. Wang. “Structures of Platinum Clusters : Planar or Spherical?” In: *Journal of Physical Chemistry A* 108 (2004), pp. 8605–8614.

[30] V. Kumar and Y. Kawazoe. “Evolution of Atomic and Electronic Structure of Pt Clusters: Planar, Layered, Pyramidal, Cage, Cubic and Octahedral Growth”. In: *Physical Review B - Condensed Matter and Materials Physics* 77.20 (2008), pp. 205418–1–10.

[31] H. Steininger, S. Lehwald, and H. Ibach. “Adsorption of Oxygen on Pt(111)”. In: *Surface Science* 123 (1982), pp. 1–17.

[32] J. Roques and A. B. Anderson. “Pt3Cr(111) Alloy Effect on the Reversible Potential of OH(ads) formation from O2 (ads) Relative to Pt(111)”. In: *Journal of Fuel Cell Science and Technology* 2.2 (2005), pp. 86–93.

[33] A. Groß. “Reactions at Surfaces Studied by Ab Initio Dynamics Calculations”. In: *Surface Science Reports* 32 (1998), pp. 291–340.

[34] C. Hartnig, P. Vassilev, and M.T.M. Koper. “Ab Initio and Classical Molecular Dynamics Studied of Electrode Reactions”. In: *Electrochimica Acta* 48 (2003), pp. 3751–3758.

[35] R. Car and M. Parrinello. “Unified Approach for Molecular Dynamics and Density-Functional Theory”. In: *Physical Review Letters* 55.22 (1985), pp. 2471–2471.

[36] S. Suwannawong, K. Doi, and S. Kawano. "Theoretical Study on Current-Voltage Characteristics of Oxygen Reduction Reaction near Platinum Surfaces". In: *International Journal of Chemical Engineering and Applications* 6.105 (2015), pp. 237–242.

[37] Y. Wang and P. B. Balbuena. "Role of Ptoton and Electric Field in the Electroreduction of O_2 on Pt(111) Surfaces: Results of an Ab-Initio Molecular Dynamics Study". In: *Journal of Physical Chemistry B* 108.14 (2004), pp. 4376–4384.

[38] Y. Wang and P. B. Balbuena. "Ab Initio Molecular Dynamics Simulations of the Oxygen Reduction Reaction on a Pt(111) Surface in the Presence of Hydrated Hydronium $(H_3O)^+(H_2O)_2$: Direct or Series Pathway". In: *Journal of The Electrochemical Society* 151.12 (2005), A2016–A2027.

[39] Y. Suzuki and K. Yamashita. "Real-time Electron Dynamics Simulation of the Adsorption of an Oxygen Molecule on Pt and Au Clusters". In: *Chemical Physics Letters* 486 (2010), pp. 48–52.

[40] R. Li et al. "Insights into the Adsorption of Oxygen and Water on Low-index Pt Surfaces by Molecular Dynamics Simulations". In: *New Journal of Chemistry* 38 (2014), pp. 683–692.

[41] Y. Okamoto. "First-principles Molecular Dynamics Simulation of O_2 Reduction on Nitrogen-doped Carbon". In: *Applied Surface Science* 256 (2009), pp. 335–341.

[42] C. Carbogno et al. "O_2 Adsorption Dynamics at Metal Surfaces: Non-adiabatic Effects, Dissociation and Dissipation". In: *Springer Series in Surface Sciences* 50 (2013), pp. 389–419.

[43] X. Hu et al. "Adsorption and Activation of O_2 on Nitrogen-doped Carbon Nanotubes". In: *Journal of Physical Chemistry C* 114.21 (2010), pp. 9603–9607.

[44] G. B. Bacskay. "A Quadratically Convergent Hartree-Fock (QC-SCF) Method. Application to Closed Systems". In: *Chemical Physics* 61 (198), pp. 385–404.

[45] J. M. Tao et al. "Climbing the Density Functional Ladder: Nonempirical Meta-generalized Gradient Approximation Designed for Molecules and Solids". In: *Physical Review Letters* 91 (2003), p. 146401.

[46] F. Weigend and R. Ahlrichs. "Balanced Basis Sets of Split Valence, Triple Zeta Valence and Quadruple Zeta Valence Quality for H to Rn: Design and Assessment of Accuracy". In: *Physical Chemistry Chemical Physics* 7 (2005), pp. 3297–3305.

[47] D. Andrae et al. "Energy-adjusted Ab Initio Pseudopotentials for the Second and Third Row Transition Elements". In: *Theoretica Chimica Acta* 77 (1990), pp. 123–141.

[48] T. H. Dunning Jr. and P. J. Hay. "Modern Theoretical Chemistry". In: ed. by H. F. Schaefer III. Vol. 3. Plenum, New York, 1977, pp. 1–28.

[49] P. J. Hay and W. R. Wadt. "Ab initio Effective Core Potentials for Molecular Calculations - Potentials for the Transition-Metal Atoms Sc to Hg". In: *Journal of Chemical Physics* 82 (1985), pp. 270–283.

[50] W. R. Wadt and P. J. Hay. "Ab initio Effective Core Potentials for Molecular Calculations - Potentials for Main Group Elements Na to Bi". In: *Journal of Chemical Physics* 82 (1985), pp. 284–298.

[51] P. J. Hay and W. R. Wadt. "Ab initio Effective Core Potentials for Molecular Calculations - Potentials for K to Au including the Outermost Core Orbitals". In: *Journal of Chemical Physics* 82 (1985), pp. 299–310.

[52] L. Pauling and Jr. E.B. Wilson. *Introduction to Quantum Mechanics with Applications to Chemistry*. Dover publications, INC., 1935.

[53] L. PIELA. *Ides of Quantum Chemistry*. 1^{st}. Elsevier, 2007.

[54] K. Doi, I. Onishi, and S. Kawano. "Dissociative Adsorption of H_2 molecules on Steric Graphene surface: Ab Initio MD Study Based on DFT". In: *Computational and Theoretical Chemistry* 994 (2012), pp. 55–64.

[55] C. J. Cramer. *Essentials of Computational Chemistry : Theories and Models*. 2nd. Wiley–VCH, Inc., 2004.

[56] J. Keith and T. Jacob. "Theoretical Studies of Potential-dependent and Competing Mechanisms of the Electrocatalytic Oxygen Reduction Reaction on Pt(111)". In: *Angewandte Chemie International Edition* 49 (2010), pp. 9521–9525.

[57] T. Jacob. "The Mechanism of Forming H_2O from H_2 and O_2 over a Pt Catalyst via Direct Oxygen Reduction". In: *Fuel Cells* 6.3–4 (2006), pp. 159–181.

Chapter 5

General Conclusion

Since a significant role of electron transfer through molecular junction in various fields, numerous researchers of such a system have been studied this issue by both experimental and computational method as reviewed in Chapter 1. As well as, the background knowledge of this thesis also was provided. Hence, we developed a theoretical model to distinguish electrical conductance of molecular species in terms of current-voltage (I-V) characteristics by focusing on non-equilibrium electron transfer. Our theoretical model was developed based on quantum scheme i.e. the Heisenberg uncertainty principle and computed parameters within density functional theory as described in Chapter 2. Further computations were carried out to investigate a relationship between the orientation of dipole moment and energy levels in molecules under the external electric field. To investigate the practical system, the theoretical model were applied in analysis of tunneling current between ssDNA and Au surface as explained in Chapter 3, additionally, the dissociative adsorption which is the significant part in ORR on Pt clusters as reported in Chapter 4.

In detail, the developed model could sufficiently explain the effect of orientation of particular molecule and I–V characteristics shows the capability to distinguish the species of ssDNA owing to the conductance profile. It may be available to investigate

effects of molecular arrangements and vibrations in tunneling current measurement of ssDNA. The reliability of computation based on the polarization energy and the dipole moment has been analyzed with the variation of base ring orientations. In addition, the analysis of molecular orbital which is responding to the interaction between DNA base molecules and the metal clusters is also provided. The results show a more realistic comparison with the previous results due to considering potential barriers at the interface and screening effect.

To study for electrode reaction, firstly, the optimized system of Pt cluster has to be identified. Our result shows that the suitable structure to model the charge transfer is Pt_{12} cluster. The charge density is induced by the adsorption process and the oxygen gains the charge from the Pt cluster which can indicate the trends of physical and chemical adsorption. The *I-V* characteristics are conducted for systems varying the position and arrangement of oxygen molecule that in adsorbed state. The results can demonstrate the different orientation and reasonably explain the conductance change. The developed model is expected to study the dissociative, adsorption and other mechanism of ORR by demonstrating each transition state in electrical profiles, thus coupling with MD simulation.

Finally, since the qualitative results and continuous processes are still limited to explain by the computation within DFT alone, the electrical profiles for the continuous intermediates of ORR are introduced by effective *ab initio* approach combining with MD simulation as in the recommendation for future studies. The conductance of each static structure is evaluated and it shows correspondence to the electrochemical reaction. Principally, the electron behavior is focused hence the importance of molecular orientations and different capacitance of system illustrated by the *I-V* characteristics.

Publication List

- Peer-Reviewed Journal Articles

    1. Szarek P., Suwannawong S., Doi K. and Kawano S., Theoretical Study on Physicochemical Aspects of a Single Molecular Junction: Application to the Bases of ssDNA, *The Journal of Physical Chemistry C*, Vol. 117 (2013), pp 10809-10817.

    2. Suwannawong S., Doi K., and Kawano S., Theoretical Study on Current-Voltage Characteristics of Oxygen Reduction Reaction near Platinum Surfaces, *International Journal of Chemical Engineering and Applications*, Vol. 6 (2015), pp. 237-242.

- International Conference and award

1. Suwannwong S., Szarek P., Doi K. and Kawano S., Ab Initio Approach to Current–Voltage Characteristics of DNA Base Molecules, in *Proceeding of the 4th TSME International Conference on Mechanical Engineering*, Pattaya, Thailand, 2013.

2. Suwannawong S., Doi K., and Kawano S., Theoretical Study on Current-Voltage Characteristics of Oxygen Reduction Reaction near Platinum Surfaces, *the 3rd International Conference on Chemical Science and Engineering (ICCSE)*, December 2014, the **best paper award**.

Acknowledgements

This thesis would not have been completed without the help and support of the gentle people around me. Firstly, I would like to express my sincere gratitude to my supervisor, Prof.Satoyuki Kawano, for his support and guidance for my studies throughout the Master's and PhD courses, for his kindness, motivation, and immense knowledge.

I am very grateful to my adviser, Assoc.Prof.Kentaro Doi, for his precious advice, priceless assistance and patience. His guidance helped me in all the time of research and writing of this thesis. I could not have imagined having a better adviser and mentor for my research.

An invaluable knowledge and good support of Dr.Pawel Szarek had been important on an academic level for which I am really thankful. About one year that he worked in our group and make worthwhile work which I can continue to make this thesis completely.

Besides my adviser, I would like to thank the rest of my thesis committees, Prof.Shigenobu Ogata and Prof.Kazuyasu Sugiyama, for their insightful comments and encouragement to widen my research from various perspectives.

I would also like to thank Asst.Prof.Hirofumi Shintaku, Assoc.Prof.Itsuo Hanasaki and Asst.Prof.Tetsuro Tsuji for their help, guidance and support all the time.

I would like to acknowledge the financial, academic and technical support of Graduate school of Engineering Science at Osaka University that provide kind co-operation and contributions. I sincerely thanks to Ministry of Education, Culture,

Sports, Science and Technology (MEXT), Japan and Thai-Nichi Institute of Technology for providing financial support to study at Osaka University.

I thank my fellow lab members for the seminar discussions, for amazing events and lab trip that I never expect to do in Japan, for the sleepless nights we were working together before deadlines, and for all the fun we have had in the last five years. I am grateful to Mr.Weixin Qian, Mr.Ryosuke Nii, Mr.Yoichi Maeda, Mr.Shoji Tanaka, Ms.Ayako Yano, Mr.Ryo Nagura, Mr.Shuto Onitsuka, Mr.Yoji Kataoka, Mr.Kanji Kawashima, Mr.Kosuke Kozai, Mr.Sho Saita, Ms.Aishah Mahmoud, Ms.Asuka Nakayama and Ms.Fumika Nito for precious friendship. And I thanks タッキー, 山P, many mangas and animations for being my inspiration to come to Japan and move on until the end.

Last, but not least, I really thank all my friends at Thailand and Japan for their cheerfulness and counsels. Above all, I am most grateful to my family and my parents for their intangible personal support, encouragement and great patience at all five years.